Chapter 3

Bridged Nucleic Acid ASOs over Locked Nucleic Acid ASOs and their impact on the structure and stability of ASO/RNA duplexes

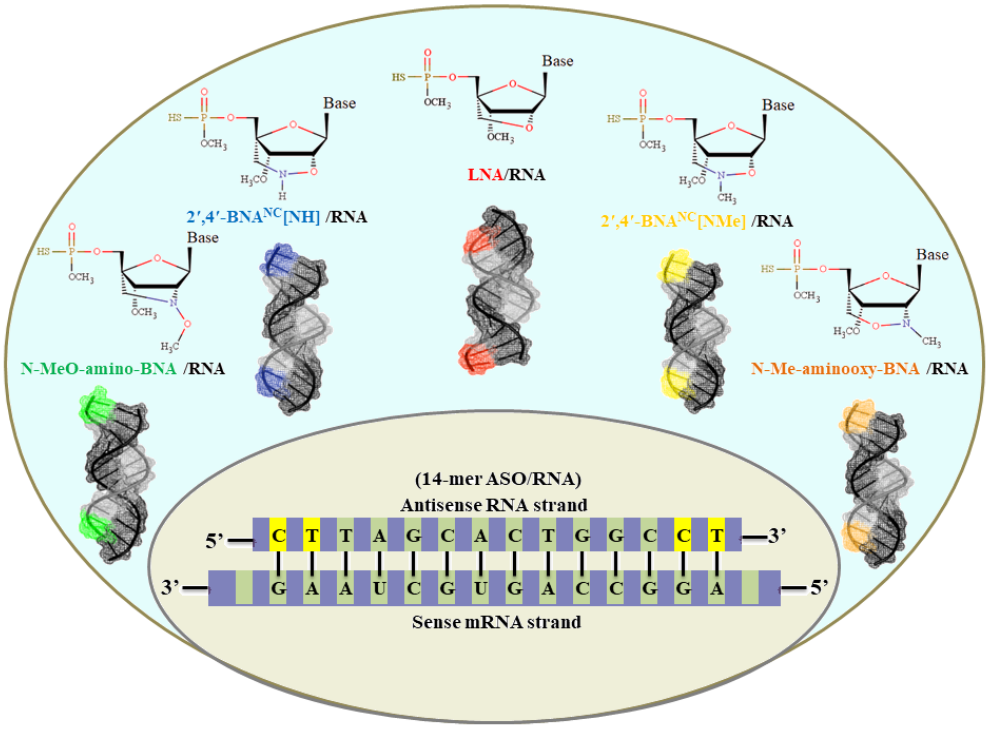

3.1. Introduction

Genetic diseases are an implication of deviation from the typical DNA sequence, either in whole or in part. A defective genetic sequence produces a flawed mRNA. Because mRNAs encode for all cellular proteins, drugs targeting faulty mRNAs are thus an optimal choice to interfere directly at the production level before they are decoded to disease causing proteins. Antisense-mRNA drugs are designed to bind sequence specifically and target complementarily to their sense-mRNAs, inhibit the production of diseases causing proteins and thereby modulate their gene expressions [1-3]. Unlike the small drug molecules and monoclonal antibodies, antisense oligonucleotides (ASOs) are a class of synthetic drug macromolecules that target not the proteins but the mutated mRNAs treating the diseases the scientific community considers difficult to be treated by small drug molecules [4-6]. Antisense medications thus have the potential to treat a wide range of diseases, revolutionizing the way treatments are found, developed, and produced on a scale uncommon in the traditional pharmaceutical sector.

Since the discovery of antisense molecules, research into therapeutic use of synthetic antisense oligonucleotides (ASOs) to treat various diseases has advanced very quickly [7-9]. Over the past few years there have been a sharp rise in the number of antisense medications entering into phase III clinical trials as a result of the expanding research on antisense molecules and their processes. Several antisense medications have received FDA approval for the treatment of breast cancer, cardiovascular disorders, and a variety of infectious and inflammatory diseases [10-13]. Today, specifically crafted medications based on antisense technology are used to treat a wide range of disorders, many of which cannot be treated with the available traditional pharmacological technologies [14-15].

Nevertheless, for successful clinical application, the modified ASOs should possess high resistance to endonucleases, high affinity for target complementary RNA sequences and bind by *Watson-Crick* base pairing forming ASO/mRNA duplexes along with excellent RNA selectivity. The cellular endonuclease RNase H is activated by the ASO/mRNA duplexes which then specifically cleaves the RNA strand from the ASO/mRNA duplexes in a targeted manner [16-17]. However, the ASOs are degraded prior to duplexing due to their limited stability in biological media and hence they must undergo thorough chemical alterations to impart a genuine antisense response. Early on, minimally modified antisense molecules wherein the phosphodiester backbone of the

nucleotides, altered by replacing one of the non-bridging oxygen atoms by sulphur (phosphorothioate-PS) were used as active ASOs [18-19]. The first antisense drug approved by the FDA was a phosphorothioate oligonucleotide marketed under the brand name "Vitravene" (ISIS-2922) in 1998 for the treatment of cytomegalovirus induced retinitis [10]. Cleavage of the duplexes by RNase H is the most desirable antisense mechanism and the PSs were able to induce the desired catalytic effect. Even so, in some cases, binding affinity and specificity to the target sequences of the PSs were less satisfactory. Thus, substitution by methylphosphonates and phosphoramidates also gained significant attention, however, PSs have remained the most successful till date [20-22]. These compounds were termed as the first-generation antisense modifications, the drawbacks of which were compensated by the second-generation antisense modifications representing alkyl modifications at the 2′-O position of the ribose sugar. Of these the most successful were the 2′-O-methyl (OMe) and 2′-O-methoxyethyl (MOE) modifications with enhanced binding affinity [23-24]. To avail outmost benefit, both first- and second-generation antisense modifications were combined to generate chimeric ASOs which could improve the nuclease resistance as well as target binding affinity. Many such chimeric gapmers are available in the market as FDA approved drugs, where both PS and MOE modifications are being used [25-28]. With the objective of obtaining better antisense modifications compared to the PS's and MOE's, third generation antisense modifications like Peptide Nucleic Acids (PNAs), Locked Nucleic Acids (LNAs), Bridged Nucleic Acids (BNAs), Morpholino oligonucleotides (PMO) *etc.* were developed [29-32]. With enhanced thermodynamic stability, nucleic acid recognition, aqueous solubility, superior hybridizing affinity, sequence selectivity and improved bio-stability compared to that of natural oligonucleotides, LNA have proven as one of the most efficient members of the newer generation antisense modifications [33-35]. However, some of its kinds were hepatotoxic, comparative nuclease resistance being found to be significantly lower than the PS's and fully modified LNA constructs or with consecutive LNA units resulted in inefficient or sometimes total failure of triplex formation [36]. By optimizing the structural elements of MOEs and LNAs and also by reducing the ASO length (from 20-mer to 14-mer), the potency of MOE based ASOs in animals was increased 3- to 5-fold ($ED_{50} \approx$ 2-5 mg/kg) without producing hepatotoxicity [37-38]. Thus, continuous efforts to engineer the LNA structure have resulted in the development of BNAs as potent LNA analogues. After all these years of development,

the 2′,4′-BNA^{NC} analogues: 2′,4′-BNA^{NC}[NH], 2′,4′-BNA^{NC}[NMe], N-Me-aminooxy BNA and N-MeO-amino BNA modifications have been found to be very promising in antisense technology [39-40]. Compared to LNAs, BNAs are highly nuclease resistant, at times even higher than the PSs. Along with higher sequence selective binding affinity for complementary RNAs, stable triplex-forming characters, they were also found to possess excellent single-mismatch discriminating ability. *In-vivo* and *in-vitro* studies showed that compared to the MOE ASOs, optimized BNA ASOs provided increased thermal stability and improved *in-vitro* activity, along with >5-fold improved *in-vivo* activity. Toxicity parameters like the AST, ALT, liver, kidney, body weights, were also found to be normal. These results suggest that chimeric gapmers with 2′,4′-BNA^{NC}[NH], 2′,4′-BNA^{NC}[NMe], N-Me-aminooxy BNA and N-MeO-amino BNA modifications can be potential drug candidates for applications in the antisense drug discovery platforms.

Interpreting the underlying chemistry of the LNA, BNA antisense modifications would help one in understanding their structural and functional significance in exhibiting higher binding affinity with higher hepato-toxicity, mechanism of action as well as guide in postulating superior antisense derivatives. However, to develop better antisense modifications detailed information on the various existing antisense modifications is very much necessary, which is limited indeed. Quantum chemical studies on a few antisense modifications like cyclohexyl PNA, MOE and LNA have been reported with no such reported study on BNA antisense modifications [41-47]. Thus, the current study aims to investigate four such BNA antisense modifications both at the molecular and oligomer level. Since PSs can induce the RNase H functions, all the modifications were further implemented with the PS backbone linkage. Oligomer hybrid duplex stability and gene silencing potential of the ASOs are described by performing a detailed classical MD simulation study on 14-mer ASO/RNA duplex gapmers, the ASO strand containing the PS-LNA, PS-BNA antisense modifications targeting the protein PTEN mRNA nucleic acid sequence. Replica copies of simulations were performed each simulated for 1 μs simulation time to account for the statistical variations obtained during MD simulations. Force-field parameters were built for all the LNA, BNA, PS-LNA, PS-BNA monomer nucleotides considered for the simulation studies. This research will assist in comparing the structure-activity relationship of the LNA, BNA antisense modifications and development of a systematic DFT & MD method-based paradigm for designing beneficial antisense modifications tuned for specific requirements.

3.2. Materials and Methods

Starting structures of 2′,4′-BNA^{NC}[NMe] monomer nucleotides containing pyrimidine nucleobases 5-methylcytosine and thymine were collected from the NMR-crystal structure of a 2′,4′-BNA^{NC}[NMe] contained 9-mer gapmer in complex with a target complementary RNA [48].

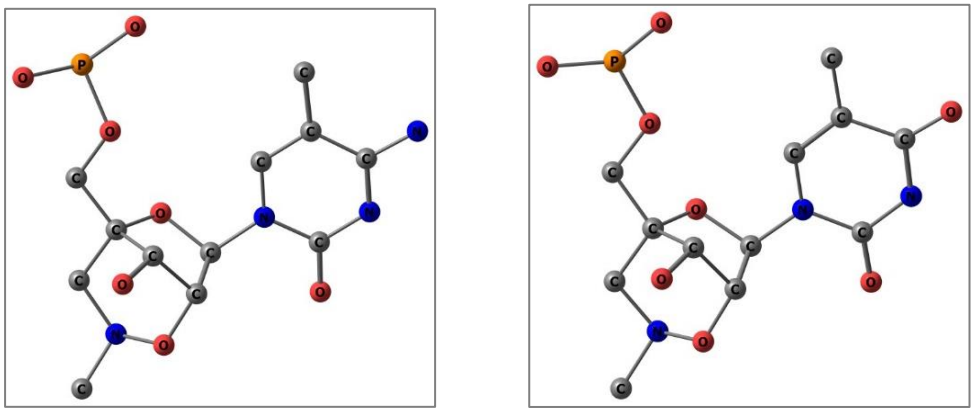

(a) NCU: 2′,4′-BNA^{NC}[NMe], 5-Methylcytosine (b) NTT: 2′,4′-BNA^{NC}[NMe], Thymine

Structures of the remaining modifications LNA, N-MeO-amino-BNA, 2′,4′-BNA^{NC}[NH] and N-Me-aminooxy-BNA were then built on the 2′,4′-BNA^{NC}[NMe] monomer nucleotides using the molecular building and visualization tools Gauss View and Discovery Studio [49-50]. In all the modifications, the 2′-carbon and 4′-carbon of the sugar moiety are linked by five different conformationally constrained functional groups each containing nucleobases Adenine(A), Guanine(G), 5-Methylcytosine(C) and Thymine(T). The same were further implemented considering the first-generation antisense modification where one of the non-bridging oxygen atoms from the sugar-phosphate backbone was replaced by Sulphur (PS backbone linkage). Schematic 2D structures of the titled LNA, BNA, PS-LNA, PS-BNA antisense modifications each containing nucleobases Adenine (A), Guanine (G), 5-Methylcytosine (C) and Thymine (T) are given in Figure 3.1 and the modification details are listed in Table 3.1.

The entire methodology of the present work includes: First, Density Functional Theory (DFT) based quantum chemical study to obtain the most stable conformations of the titled LNA, BNA and PS-LNA, PS-BNA monomer nucleotides followed by quantum chemical descriptor derivation for the same. Second, generation of force-field parameters of all the LNA, BNA, PS-LNA, PS-BNA monomer nucleotides corresponding to the four nucleobases followed by a detailed MD simulation study on 14-mer ASO/RNA duplex

gapmers incorporating the PS-LNA, PS-BNA antisense modifications targeting the protein PTEN mRNA nucleic acid sequence with replica copies MD simulations accounting two data sets, each simulated for 1 μs simulation time.

3.2.1. Density Functional Theory (DFT) Calculations

DFT based quantum chemical calculations were performed to obtain optimized structures and ground state energies of the titled LNA, BNA, PS-LNA, PS-BNA monomer nucleotides using the Gaussian09 software package [49]. Full geometry optimization along with frequency calculations were done employing the meta-GGA, hybrid, unrestricted M06-2X functional alongside triple-ζ split valence and diffused basis set 6-311G(d,p) for all atoms, without imposing any symmetry constraints [51-53]. Using the conductor-like polarizable continuum solvation model (CPCM) water (with dielectric constant 78.39) was added for implicit solvation [54]. Natural Bond Orbital (NBO) calculations were performed on the optimized structures at the same level of theory to generate wave function files. Molecular orbital (MO) composition analysis was carried out to find out the composition of the HOMO-LUMO iso-surfaces using the open source Multiwfn software program [55].

3.2.1.1. Global reactivity descriptors

According to the *Koopmans'* theorem, IP and EA values are described as the negative of energy *eigenvalues*, where IP = $-E_{HOMO}$ and EA = $-E_{LUMO}$, respectively. These fundamental equations under the framework of DFT are used to analyse a set of global quantities that describe the structural changes from one ground-state to another.

The global reactivity descriptors global hardness (η), global softness (S), chemical potential (μ) and electrophilicity (ω) all were calculated using the equations described below [56-58].

$$\text{Global hardness } (\eta) = (\text{IP} - \text{EA}) / 2$$

$$\text{Global softness (S)} = {}^{1}/_{2\eta}$$

$$\text{Chemical potential } (\mu) = -(\text{IP} + \text{EA}) / 2$$

$$\text{Electrophilicity } (\omega) = {}^{\mu^2}/_{2\eta}$$

3.2.2. Molecular Dynamics (MD) Simulations

3.2.2.1. System building and Force-field parameters

Force-field parameters were developed for all the LNA, BNA, PS-LNA, PS-BNA monomer nucleotides using the parameterization protocol given in literature [59-60]. The optimised structures obtained from the DFT calculations were considered for RESP charge fitting, carried out using the *antechamber* module of AMBER. Partial atomic charges were derived at the M06-2X/6-311G** level of theory by using the Gaussian09 program package [49]. RESP charge fitting was done using the ANTECHAMBER module of AMBER18 [61]. Parameters for PS backbone has also been reported by Orozco's group [62]. After derivation of RESP charges the *prepc* files were developed using the *prepgen* module of AMBER. However, these *prepc* files were further modified matching the atom types and atom sequence order with the atom types and atom sequence order of DNA.OL15 and RNA.OL3 force-fields. These *prepc* files were then used to generate the *frcmod* files using the *parmchk2* module of AMBER. Thus, the force-field parameters were built in a way mimicking the force-field parameters of the standard nucleic acids making them compatible with the traditional DNA, RNA force-fields.

Post-parameterization, a set of 14-mer (5′-CTTAGCACTGGCCT-3′/3′-GAAUCGUGACCGGA-5′) ASO/RNA duplex gapmers, the 5′-CTTAGCACTGGCCT-3′ ASO strand was built by incorporating the PS-LNA, PS-BNA antisense modifications. The modifications were incorporated selectively at the two 5′ and 3′ end residues of the ASO strand assimilating into a duplex gapmer. On the contrary, non-terminal residues from the ASO strand (5′-~~CT~~TAGCACTGGC~~CT~~-3′) are phosphorothioate nucleotides (PS-DNAs) yielding ASO-(PS-DNA)-ASO/RNA duplex gapmers. The 3′-AGGCCAGUGCUAAG-5′ strand has been considered as target complementary RNA strand. The regular DNA/RNA hybrid has been considered as the control system for comparison.

Thus, the six iso-sequential hybrid duplexes include 14-mer duplex gapmers (a) DNA/RNA (b) PS-LNA/RNA (c) PS-N-MeO-amino-BNA/RNA. (d) PS-2′,4′-BNA^{NC}[NH]/RNA (e) PS-2′,4′-BNA^{NC}[NMe]/RNA and (f) PS-N-Me-aminooxy-BNA/RNA. The systems were charge neutralized by adding Na^+/Cl^- as counter ions and solvated with TIP3P water box for explicit solvation [63]. The entire duplex building

process was carried out using the leap module of AMBER implementing the standard force field parameters 'DNA.OL15' for DNA, 'RNA.OL3' for RNA nucleobases [64-65] and the in-house generated force-field parameters for the LNA, BNA and PS-LNA, PS-BNA antisense modifications.

3.2.2.2. Simulation Protocol and Trajectory Analysis

Simulations were carried out using the all-atom classical MD simulation framework of AMBER18. Replica copies of MD simulations were performed accounting to two data sets (Set-I & Set-II) each simulated for 1 μs simulation time, to consider the statistical variance observed in the calculations. To obtain proper initial structures, the systems were energy minimized using the steepest descent method for 5000 steps, followed by 5000 steps conjugate gradient method. Energy minimization was performed keeping the solute atoms fixed using constraints of 100 kcal/mol initially, then gradually reducing and finally removing the constraints on all the solute atoms. The systems were then heated slowly from 0 K to 300 K canonical ensemble by using constraints of 100 kcal/mol on all the solute atoms. Post heating, the systems underwent equilibration in a similar way by gradually reducing the constraints and finally removing the constraints on all the solute atoms in an isothermal isobaric (NPT) ensemble.

Simulations were performed under periodic boundary conditions by employing the Particle Mesh Ewald technique to account for the long-range electrostatics [66]. MD integration was carried out using a 2.0 fs time step, employing the SHAKE algorithm on all the bonds involving hydrogen atoms [67]. For non-bonding interactions, a cut-off distance of 10 Å has been used. The pair-list was updated at every 1000 steps. NPT conditions were maintained throughout the production simulation run. The systems were then allowed to simulate under production run conditions for 1 μs simulation time and the trajectories were used for analysis. Two sets of simulations were carried out each set corresponding to 1 μs simulation time to account for the statistical variations obtained during MD simulations.

The CPPTRAJ module of Amber Tools was used to calculate the RMSD, RMSF, sugar pucker, inter- and intra-strand phosphate distances and base pairing H-bonds [68]. Solvent accessible surface area (SASA) was also calculated for all the duplexes using the CPPTRAJ module [69]. MMGBSA module of AMBER18 was used for calculating the free energy of all the duplexes [70-71].

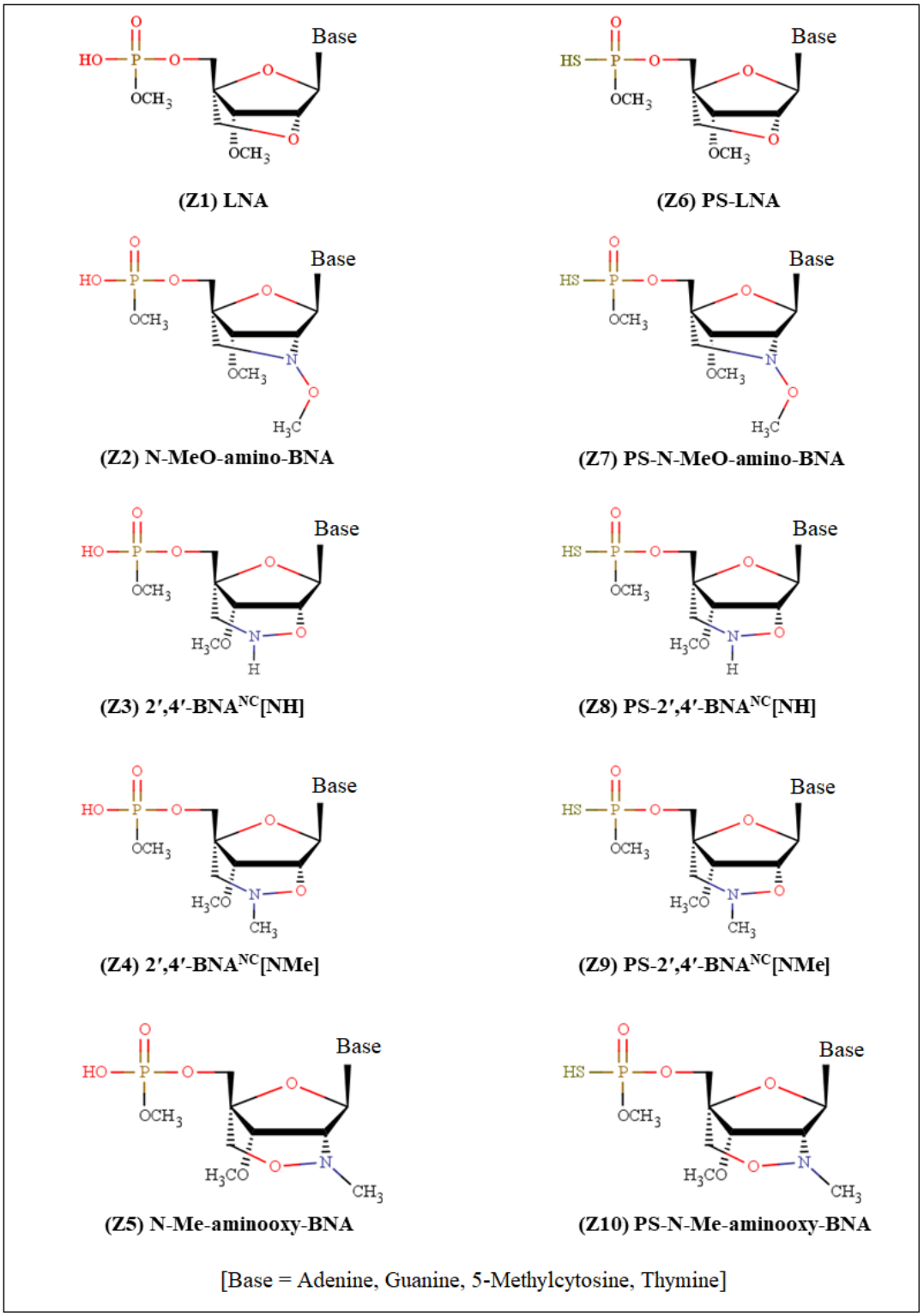

Figure 3.1: Schematic 2D representation of LNA; N-MeO-amino-BNA; 2′,4′-BNA^{NC}[NH]; 2′,4′-BNA^{NC}[NMe]; N-Me-aminooxy-BNA antisense modifications holding normal phosphate backbone (Z1-Z5) and PS-LNA; PS-N-MeO-amino-BNA; PS-2′,4′-BNA^{NC}[NH]; PS-2′,4′-BNA^{NC}[NMe]; PS-N-Me-aminooxy-BNA antisense modification holding phosphorothioate (PS) backbone (Z6-Z10) each containing nucleobases Adenine (A), Guanine (G), 5-Methylcytosine (C) and Thymine (T) respectively.

Table 3.1: Modification details of LNA; N-MeO-amino-BNA; 2′,4′-BNA^{NC}[NH]; 2′,4′-BNA^{NC}[NMe]; N-Me-aminooxy-BNA antisense modifications holding normal phosphate backbone (Z1-Z5) and PS-LNA; PS-N-MeO-amino-BNA; PS-2′,4′-BNA^{NC}[NH]; PS-2′,4′-BNA^{NC}[NMe]; PS-N-Me-aminooxy-BNA antisense modifications holding phosphorothioate (PS) backbone (Z6-Z10) each containing nucleobases Adenine (A), Guanine (G), 5-Methylcytosine (C) and Thymine (T) along with the name codes used in the present work.

Nucleobases	Name Code	Modification Details	Name Code	Modification Details
Adenine (A)	A-Z1	(Z1) LNA	A-Z6	(Z6) PS-LNA
	A-Z2	(Z2) N-MeO-amino-BNA	A-Z7	(Z7) PS-N-MeO-amino-BNA
	A-Z3	(Z3) 2′,4′-BNA^{NC}[NH]	A-Z8	(Z8) PS-2′,4′-BNA^{NC}[NH]
	A-Z4	(Z4) 2′,4′-BNA^{NC}[NMe]	A-Z9	(Z9) PS-2′,4′-BNA^{NC}[NMe]
	A-Z5	(Z5) N-Me-aminooxy-BNA	A-Z10	(Z10) PS-N-Me-aminooxy-BNA
Guanine (G)	G-Z1	(Z1) LNA	G-Z6	(Z6) PS-LNA
	G-Z2	(Z2) N-MeO-amino-BNA	G-Z7	(Z7) PS-N-MeO-amino-BNA
	G-Z3	(Z3) 2′,4′-BNA^{NC}[NH]	G-Z8	(Z8) PS-2′,4′-BNA^{NC}[NH]
	G-Z4	(Z4) 2′,4′-BNA^{NC}[NMe]	G-Z9	(Z9) PS-2′,4′-BNA^{NC}[NMe]
	G-Z5	(Z5) N-Me-aminooxy-BNA	G-Z10	(Z10) PS-N-Me-aminooxy-BNA
5-Methyl cytosine (C)	C-Z1	(Z1) LNA	C-Z6	(Z6) PS-LNA
	C-Z2	(Z2) N-MeO-amino-BNA	C-Z7	(Z7) PS-N-MeO-amino-BNA
	C-Z3	(Z3) 2′,4′-BNA^{NC}[NH]	C-Z8	(Z8) PS-2′,4′-BNA^{NC}[NH]
	C-Z4	(Z4) 2′,4′-BNA^{NC}[NMe]	C-Z9	(Z9) PS-2′,4′-BNA^{NC}[NMe]
	C-Z5	(Z5) N-Me-aminooxy-BNA	C-Z10	(Z10) PS-N-Me-aminooxy-BNA
Thymine (T)	T-Z1	(Z1) LNA	T-Z6	(Z6) PS-LNA
	T-Z2	(Z2) N-MeO-amino-BNA	T-Z7	(Z7) PS-N-MeO-amino-BNA
	T-Z3	(Z3) 2′,4′-BNA^{NC}[NH]	T-Z8	(Z8) PS-2′,4′-BNA^{NC}[NH]
	T-Z4	(Z4) 2′,4′-BNA^{NC}[NMe]	T-Z9	(Z9) PS-2′,4′-BNA^{NC}[NMe]
	T-Z5	(Z5) N-Me-aminooxy-BNA	T-Z10	(Z10) PS-N-Me-aminooxy-BNA

3.3. Results and Discussion

3.3.1. DFT Results

3.3.1.1. Structure and Energetics of LNA, BNA, PS-LNA, PS-BNA monomer nucleotides

LNAs are derivatives of RNAs in which the ribose sugar ring is locked by a methylene bridge that connects the 2′-oxygen with the 4′-carbon of the ribose sugar ring. The bridge results into a *C3′-endo* sugar puckering geometry reducing conformational flexibility of the ribose and increasing local organization of the phosphate backbone. The LNA antisense modifications although have been reported to have stronger binding properties, they bear a higher toxicity profile compared to MOE antisense modifications [36].

BNAs are structural extensions of LNAs, bridged by a wide variety of chemically modified functional groups, originally developed to improve the drawbacks of existing LNAs. To study the LNA, BNA antisense modifications their characteristic structural and electronic properties were investigated to understand the chemistry behind them imparting finer antisense consequences, which can be further modified into better antisense modifications on demand.

The investigation underway consists of both purine and pyrimidine motifs of LNA, N-MeO-amino-BNA, 2′,4′-BNA^{NC} analogues: 2′,4′-BNA^{NC}[NH], 2′,4′-BNA^{NC}[NMe] and N-Me-aminooxy-BNA antisense modifications. Since PSs are known to induce RNase H activity of modified ASOs, hence, the particular LNA, BNA modifications were further studied involving the PS modifications yielding PS-LNA, PS-N-MeO-amino-BNA, PS-2′,4′-BNA^{NC}[NH], PS-2′,4′-BNA^{NC}[NMe], PS-N-Me-aminooxy-BNA modifications. Physical effects of Sulphur substitution on RNA structure and dynamics have been discussed using MD simulations and high-level QM/MM calculations interpreting an H-bond, an anion-π interaction and a potassium binding site formed by RNA phosphates. The sulphur substitution, besides weakening the direct H-bond interaction, reduces the directionality of H-bonding while increasing its dispersion component of the anion-π stacking [72].

A molecular structure contains the characteristic features responsible for its physical, chemical, biological properties and quantum chemical analysis of the molecular geometries can help in determining the structure-activity relationship of related molecules. As such, the modified nucleotides were subjected to DFT based full geometry optimization followed by single-point energy calculations on the optimized structures to

evaluate their various structural and electronic properties at the monomer level. Optimized structures of the LNA, BNA monomer nucleotides holding normal phosphate backbone (Z1-Z5) and PS-LNA, PS-BNA monomer nucleotides holding PS backbone (Z6-Z10, S-conformers) calculated at the M06-2X/6-311G(d,p) level of theory are given in Figure 3.2. HOMO-LUMO energies, energy gaps, Global hardness (η), Global softness (S), Chemical potential (μ) and Electrophilicity (ω) of pristine nucleotides Adenine (A), Guanine (G), Cytosine (C) and Thymine (T) are provided now for comparative purpose in Table 3.2.

Table 3.2: The E_{HOMO}, E_{LUMO}, ΔE_{gap}, Global hardness (η), Global softness (S), Chemical potential (μ) and Electrophilicity (ω) of pristine nucleotides Adenine (A), Guanine (G), Cytosine (C) and Thymine (T) calculated at the M06-2X/6-311G(d,p) level of theory.

Name Code	E_{HOMO} (eV)	E_{LUMO} (eV)	ΔE_{gap} (eV)	η (eV)	S (eV)	μ (eV)	ω (eV)
Adenine	-7.597	0.110	7.707	3.853	0.130	-3.744	1.819
Guanine	-7.250	0.613	7.864	3.932	0.127	-3.318	1.400
Cytosine	-8.033	-0.172	7.862	3.931	0.127	-4.103	2.141
Thymine	-7.986	-0.142	7.845	3.922	0.127	-4.064	2.105

The modified nucleotides when-in complex with the RNAs should adopt an *N-type* conformation favouring the *C3'-endo* sugar puckering geometry, an important criterion for therapeutic antisense applications [73]. Results from the optimized structures clearly revealed sugar puckering of the modified nucleobases to exists in an *N-type* conformation. Further, to bind sequence specifically to their target RNAs the relative sugar-base orientation of the monomer nucleotides should exist in an *anti*-conformation, a property of *A-form* helix observed in the RNAs. The representative chi (χ) torsion angle describes the relative sugar-base orientation in standard nucleic acids which generally falls into the range of +90° to +180°/–90° to –180° (or 180° to 270°) corresponding to the *anti*-conformation in *A-form* nucleic acid duplexes [74]. Calculated chi (χ) torsion angle values of all the monomer nucleotides listed in Table 3.3 suggest their relative sugar-base orientations to be in *anti*-conformation which can adopt RNA-mimicking *A-form* helix structures and increase the strength of base-pairing and base-stacking interactions during duplex formation.

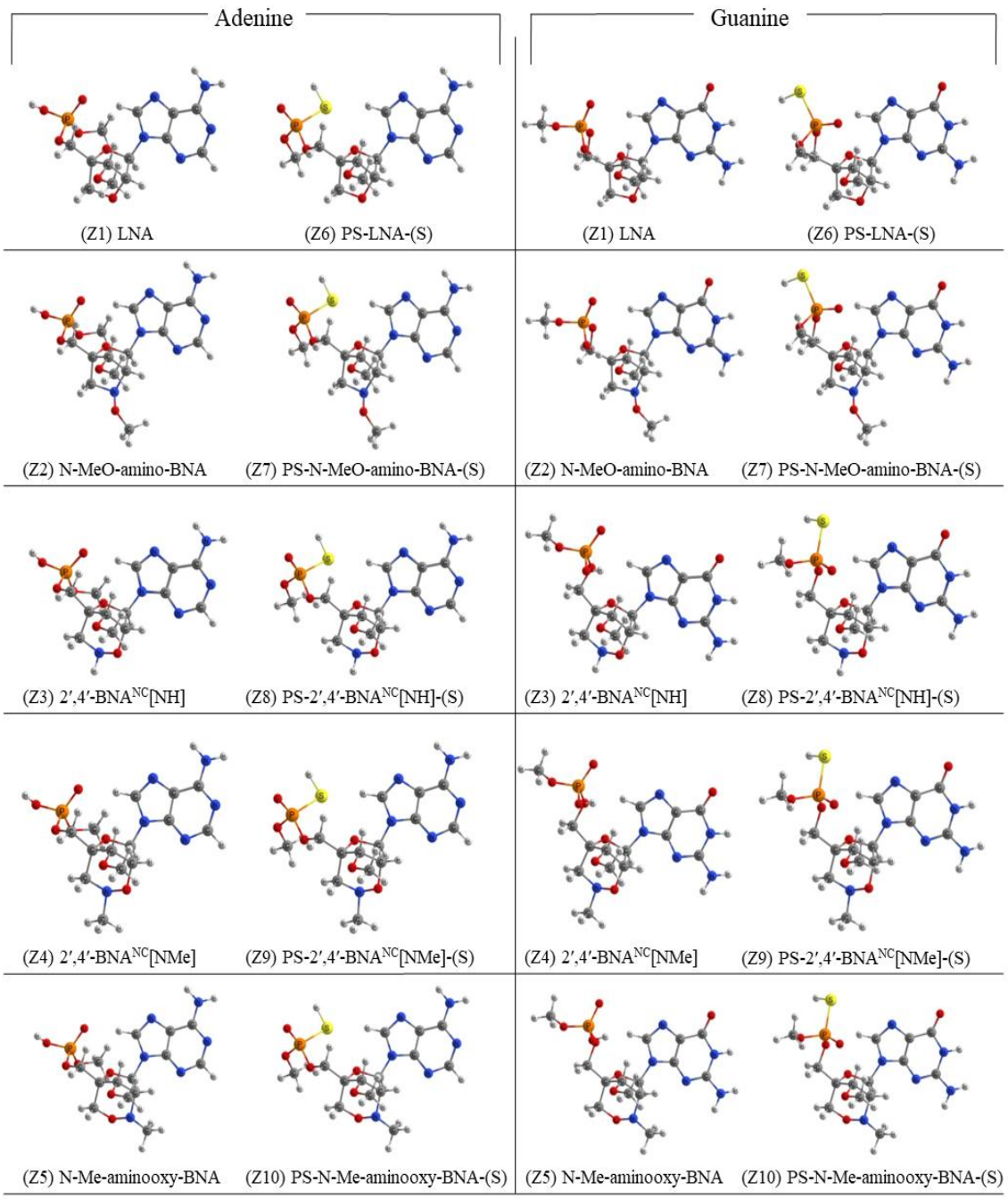

Figure 3.2: Optimized structures of LNA; N-MeO-amino-BNA; 2′,4′-BNA^{NC}[NH]; 2′,4′-BNA^{NC}[NMe]; N-Me-aminooxy-BNA monomer nucleotides holding normal phosphate backbone (Z1-Z5) and PS-LNA; PS-N-MeO-amino-BNA; PS-2′,4′-BNA^{NC}[NH]; PS-2′,4′-BNA^{NC}[NMe]; PS-N-Me-aminooxy-BNA monomer nucleotides holding phosphorothioate (PS) backbone (Z6-Z10, S conformers) each containing nucleobases Adenine (A), Guanine (G), 5-Methylcytosine (C) and Thymine (T) calculated at the M06-2X/6-311G(d,p) level of theory.

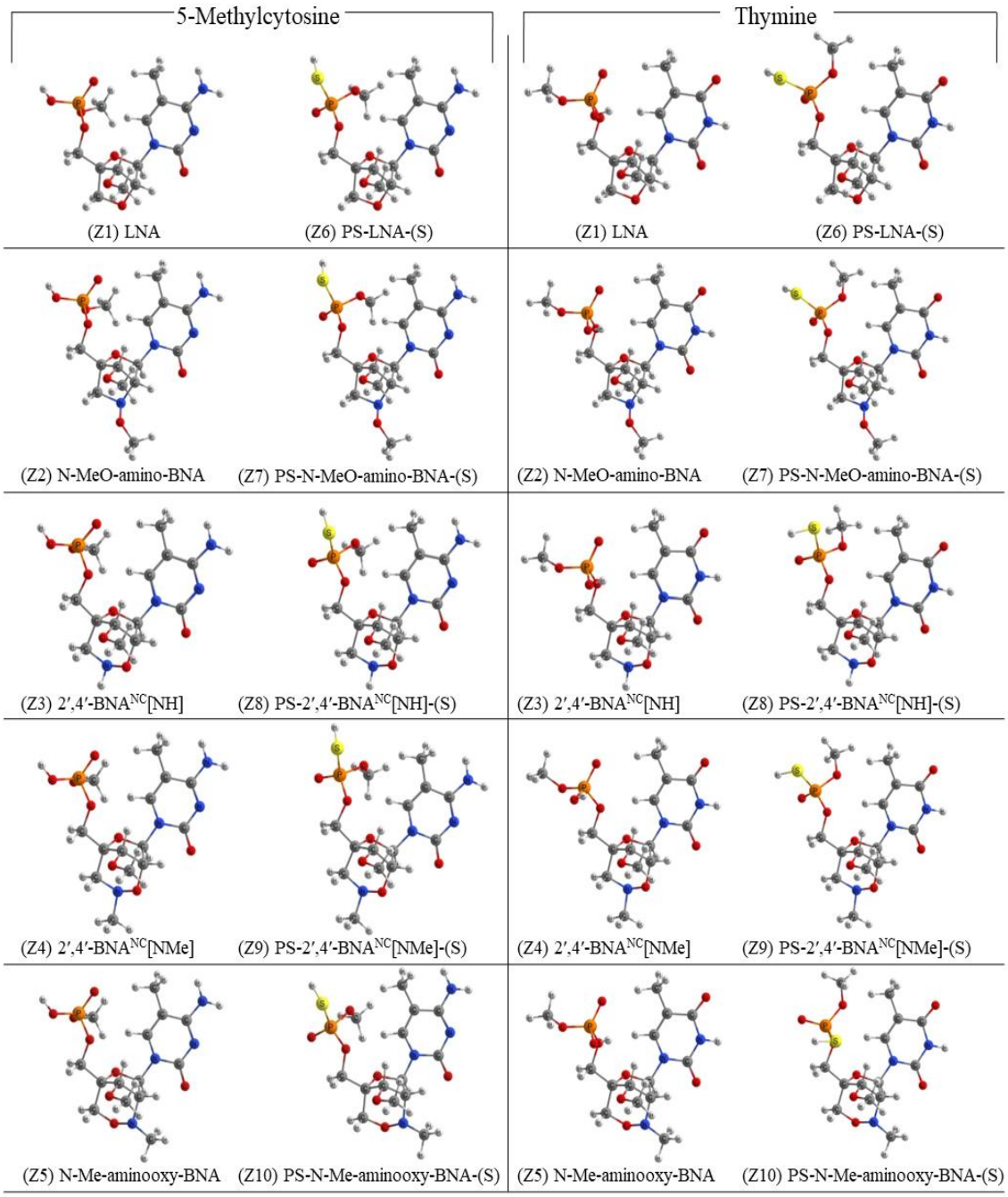

Figure 3.2: Optimized structures of LNA; N-MeO-amino-BNA; 2′,4′-BNA^{NC}[NH]; 2′,4′-BNA^{NC}[NMe]; N-Me-aminooxy-BNA monomer nucleotides holding normal phosphate backbone (Z1-Z5) and PS-LNA; PS-N-MeO-amino-BNA; PS-2′,4′-BNA^{NC}[NH]; PS-2′,4′-BNA^{NC}[NMe]; PS-N-Me-aminooxy-BNA monomer nucleotides holding phosphorothioate (PS) backbone (Z6-Z10, S conformers) each containing nucleobases Adenine (A), Guanine (G), 5-Methylcytosine (C) and Thymine (T) calculated at the M06-2X/6-311G(d,p) level of theory.

Table 3.3: The chi (χ) torsion angle, E_{HOMO}, E_{LUMO} and ΔE_{gap} of LNA; N-MeO-amino-BNA; 2′,4′-BNA^{NC}[NH]; 2′,4′-BNA^{NC}[NMe]; N-Me-aminooxy-BNA monomer nucleotides (Z1-Z5) and PS-LNA; PS-N-MeO-amino-BNA; PS-2′,4′-BNA^{NC}[NH]; PS-2′,4′-BNA^{NC}[NMe]; PS-N-Me-aminooxy-BNA monomer nucleotides (Z6-Z10, S-conformers) with their respective nucleobases Adenine (A), Guanine (G), 5-Methylcytosine (C) and Thymine (T) calculated at the M06-2X/6-311G(d,p) level of theory.

Name Code	Chi (χ)	E_{HOMO} (eV)	E_{LUMO} (eV)	ΔE_{gap} (eV)	Name Code	Chi (χ)	E_{HOMO} (eV)	E_{LUMO} (eV)	ΔE_{gap} (eV)
(A-Z1)	176.922	-7.625	0.086	7.711	(A-Z6)	179.517	-7.646	0.070	7.717
(A-Z2)	-179.350	-7.627	0.080	7.707	(A-Z7)	-177.456	-7.643	0.071	7.714
(A-Z3)	-177.949	-7.609	0.095	7.704	(A-Z8)	-174.651	-7.630	0.071	7.701
(A-Z4)	-179.083	-7.605	0.098	7.703	(A-Z9)	-172.768	-7.634	0.063	7.698
(A-Z5)	-176.749	-7.603	0.090	7.693	(A-Z10)	-173.138	-7.623	0.067	7.689
(G-Z1)	-171.877	-7.344	0.545	7.888	(G-Z6)	-165.339	-7.320	0.573	7.893
(G-Z2)	-171.087	-7.335	0.548	7.883	(G-Z7)	-167.391	-7.310	0.576	7.886
(G-Z3)	-166.604	-7.296	0.585	7.880	(G-Z8)	-166.987	-7.299	0.582	7.881
(G-Z4)	-165.076	-7.296	0.585	7.880	(G-Z9)	-166.688	-7.298	0.582	7.880
(G-Z5)	-167.932	-7.295	0.583	7.878	(G-Z10)	-168.292	-7.296	0.582	7.878
(C-Z1)	-165.801	-7.713	-0.044	7.669	(C-Z6)	-163.036	-7.719	-0.043	7.676
(C-Z2)	-164.372	-7.723	-0.036	7.688	(C-Z7)	-163.090	-7.725	-0.028	7.697
(C-Z3)	-161.379	-7.634	-0.009	7.626	(C-Z8)	-160.094	-7.640	-0.020	7.621
(C-Z4)	-161.910	-7.618	-0.010	7.608	(C-Z9)	-159.961	-7.623	-0.021	7.602
(C-Z5)	-161.493	-7.553	-0.009	7.544	(C-Z10)	-160.091	-7.559	-0.016	7.543
(T-Z1)	-166.725	-7.940	-0.131	7.809	(T-Z6)	-164.218	-7.956	-0.151	7.805
(T-Z2)	-166.787	-7.947	-0.116	7.831	(T-Z7)	-164.030	-7.953	-0.122	7.830
(T-Z3)	-162.244	-7.835	-0.099	7.736	(T-Z8)	-160.349	-7.823	-0.096	7.728
(T-Z4)	-163.090	-7.799	-0.085	7.714	(T-Z9)	-159.943	-7.796	-0.114	7.683
(T-Z5)	-163.494	-7.724	-0.103	7.621	(T-Z10)	-165.347	-7.721	-0.095	7.626

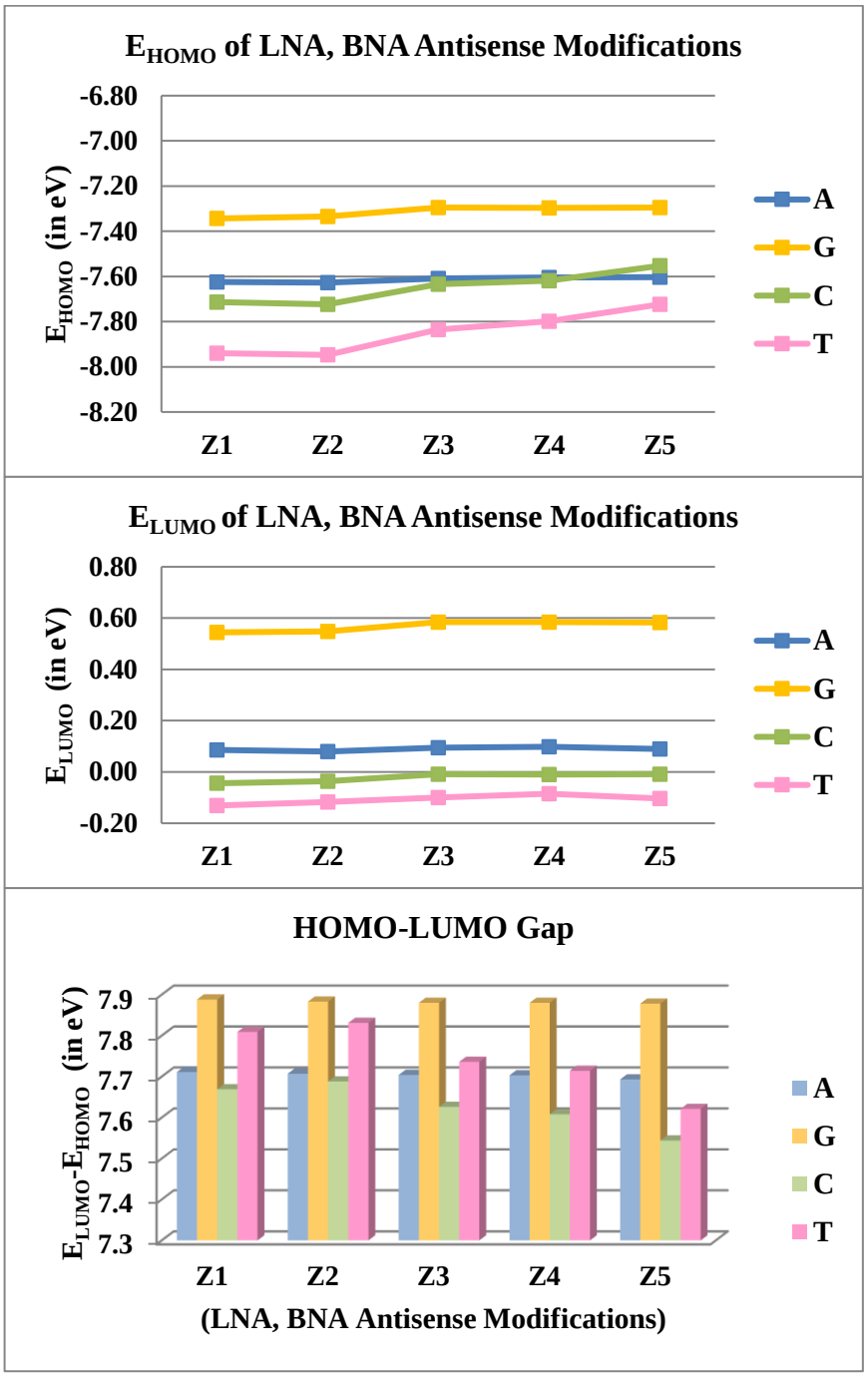

Figure 3.3: E_{HOMO}, E_{LUMO} and ΔE_{gap} of LNA; N-MeO-amino-BNA; 2′,4′-BNA^{NC}[NH]; 2′,4′-BNA^{NC}[NMe]; N-Me-aminooxy-BNA monomer nucleotides holding normal phosphate backbone (Z1-Z5) and PS-LNA; PS-N-MeO-amino-BNA; PS-2′,4′-BNA^{NC}[NH]; PS-2′,4′-BNA^{NC}[NMe]; PS-N-Me-aminooxy-BNA monomer nucleotides holding phosphorothioate (PS) backbone (Z6-Z10, S conformers) each containing nucleobases Adenine (A), Guanine (G), 5-Methylcytosine (C) and Thymine (T) calculated at the M06-2X/6-311G(d,p) level of theory.

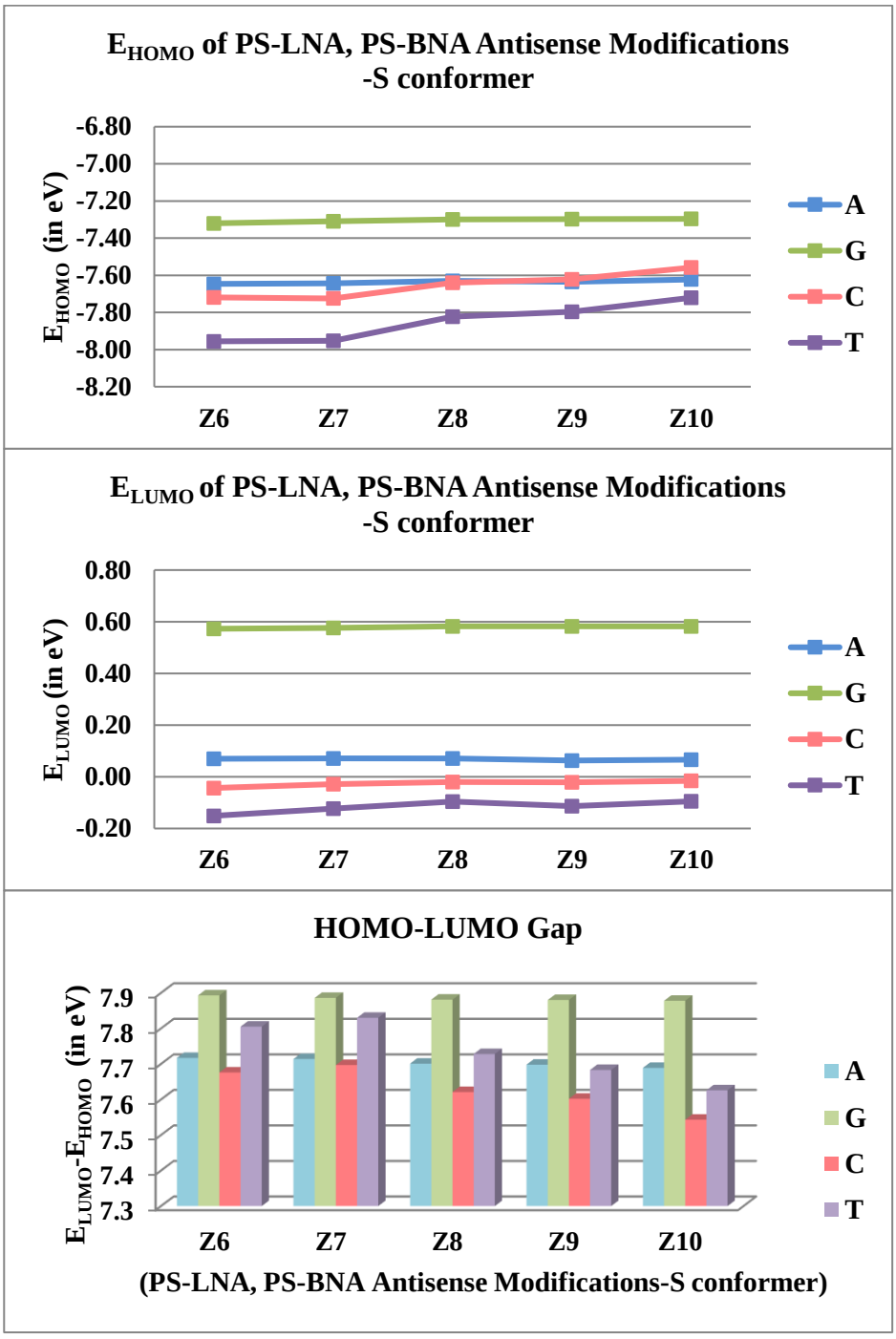

Figure 3.3: E_{HOMO}, E_{LUMO} and ΔE_{gap} of LNA; N-MeO-amino-BNA; 2′,4′-BNA^{NC}[NH]; 2′,4′-BNA^{NC}[NMe]; N-Me-aminooxy-BNA monomer nucleotides holding normal phosphate backbone (Z1-Z5) and PS-LNA; PS-N-MeO-amino-BNA; PS-2′,4′-BNA^{NC}[NH]; PS-2′,4′-BNA^{NC}[NMe]; PS-N-Me-aminooxy-BNA monomer nucleotides holding phosphorothioate (PS) backbone (Z6-Z10, S conformers) each containing nucleobases Adenine (A), Guanine (G), 5-Methylcytosine (C) and Thymine (T) calculated at the M06-2X/6-311G(d,p) level of theory.

3.3.1.2. Molecular Orbital analysis of LNA, BNA, PS-LNA, PS-BNA monomer nucleotides

HOMO-LUMO of a molecule are important quantum chemical parameters that can provide subtle information about the binding sites available within the LNA, BNA, PS-LNA, PS-BNA monomer nucleotides for interactions with host molecules. Information obtained from the HOMO energy (E_{HOMO}), the LUMO energy (E_{LUMO}) and the HOMO-LUMO energy gap (ΔE_{gap}) are thus important indicators considering the chemical reactivity and stability of the monomer nucleotides which could provide detailed information on the bonding nature of molecules. Calculated E_{HOMO}, E_{LUMO} and ΔE_{gap} of the LNA, BNA and PS-LNA, PS-BNA monomer nucleotides estimated at the M06-2X/6-311G(d,p) level of theory are listed on Table 3.3 and plotted in Figure 3.3.

In case of the LNA, BNA antisense modifications (Z1-Z5), guanine nucleobase has high lying $E_{HOMO,}$ high lying E_{LUMO} and thymine nucleobase has low lying $E_{HOMO,}$ low lying E_{LUMO} compared to the other nucleobases. Now, E_{HOMO} determines the electron donating ability of a molecule and E_{LUMO} determines the ability of the molecule to accept electrons. Higher the E_{HOMO} better is the electron donating capacity and lower the E_{LUMO} better is the electron accepting capacity. Thus, guanine nucleobases bearing the LNA, BNA modifications will be better electron donors and thymine nucleobases will be better electron acceptors, irrespective of the type of modification employed.

In case of PS-LNA, PS-BNA antisense modifications (Z6-Z10, S-conformers), again, guanine nucleobase has high lying $E_{HOMO,}$ high lying E_{LUMO} and thymine nucleobase has low lying $E_{HOMO,}$ low lying E_{LUMO} compared to the other nucleobases. Thus, guanine nucleobases bearing the PS-LNA, PS-BNA modifications will be better electron donors and accordingly thymine nucleobases will be better electron acceptors, irrespective of the type of modification employed. Accordingly, guanine nucleobase has a higher ΔE_{gap} for both the bare and the PS antisense modifications.

Molecular orbital composition of the titled LNA, BNA and PS-LNA, PS-BNA monomer nucleotides were studied by observing the orientation and configuration of their HOMO-LUMO isosurfaces, estimated at the M06-2X/6-311G(d,p) level of theory, presented in Figure 3.4. HOMO-LUMO isosurfaces of all the monomer nucleotides were majorly distributed on the nucleobase region irrespective of the type of the modification, be it the purines or pyrimidines. Being embedded within might be one of the prime reasons favouring falloff in their interactions with RNase H.

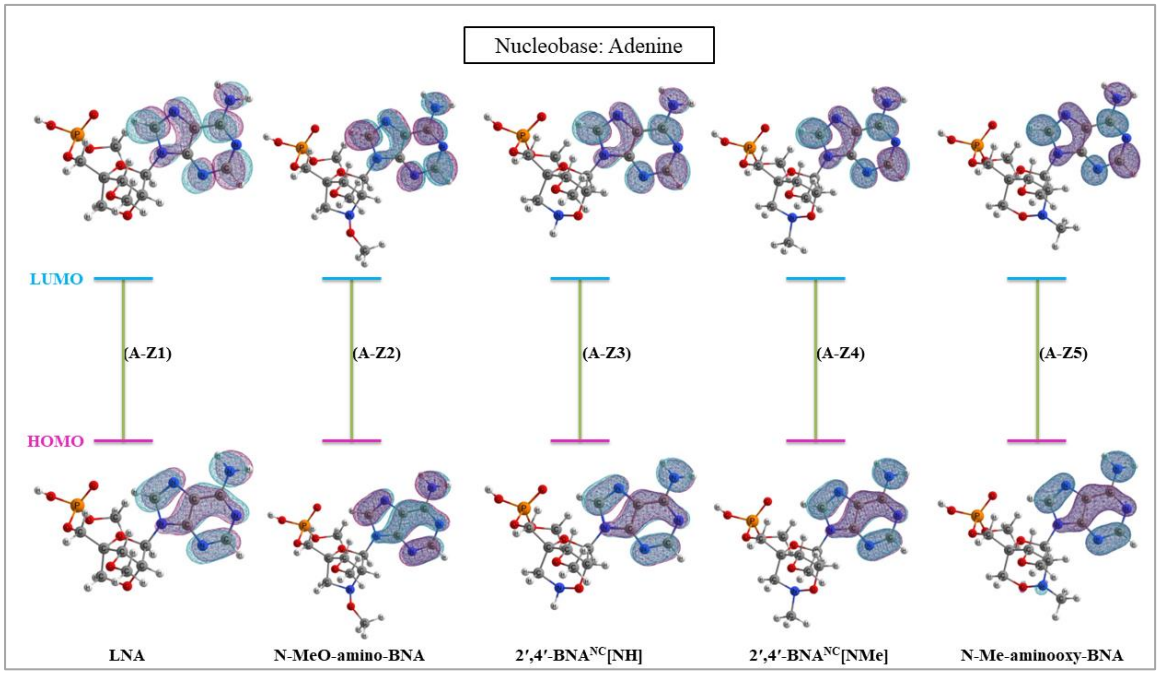
Nucleobase: Adenine
LUMO
(A-Z1)
(A-Z2)
(A-Z3)
(A-Z4)
(A-Z5)
HOMO
LNA
N-MeO-amino-BNA
2′,4′-BNA^NC[NH]
2′,4′-BNA^NC[NMe]
N-Me-aminooxy-BNA

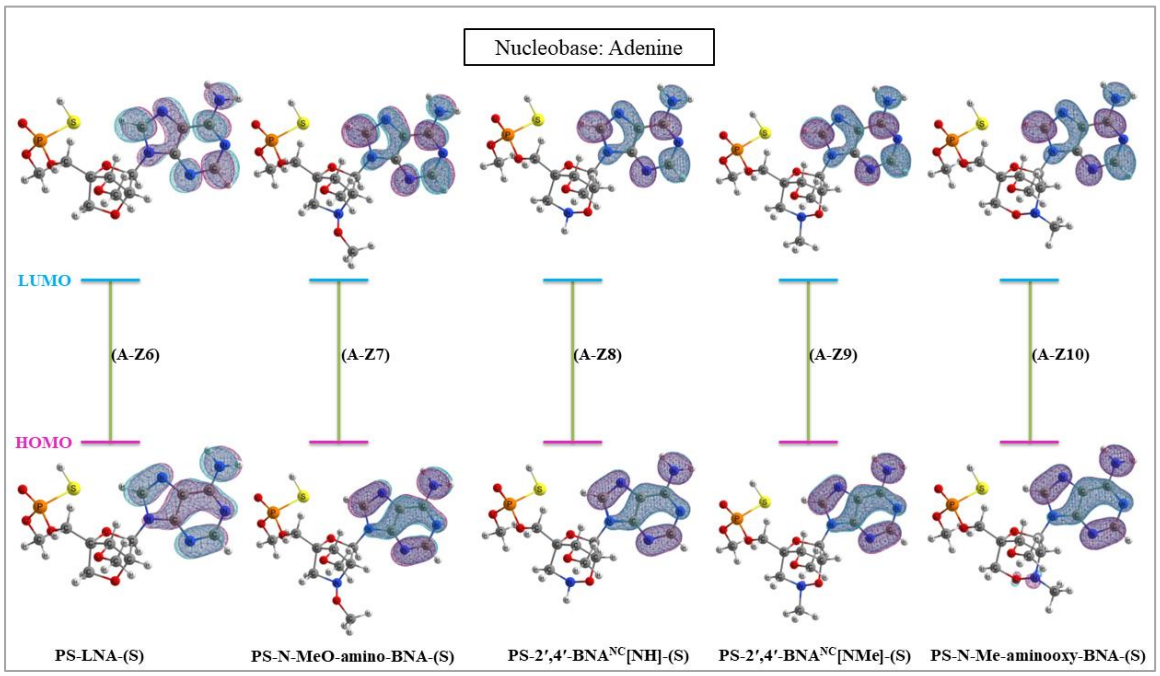
Nucleobase: Adenine
LUMO
(A-Z6)
(A-Z7)
(A-Z8)
(A-Z9)
(A-Z10)
HOMO
PS-LNA-(S)
PS-N-MeO-amino-BNA-(S)
PS-2′,4′-BNA^NC[NH]-(S)
PS-2′,4′-BNA^NC[NMe]-(S)
PS-N-Me-aminooxy-BNA-(S)

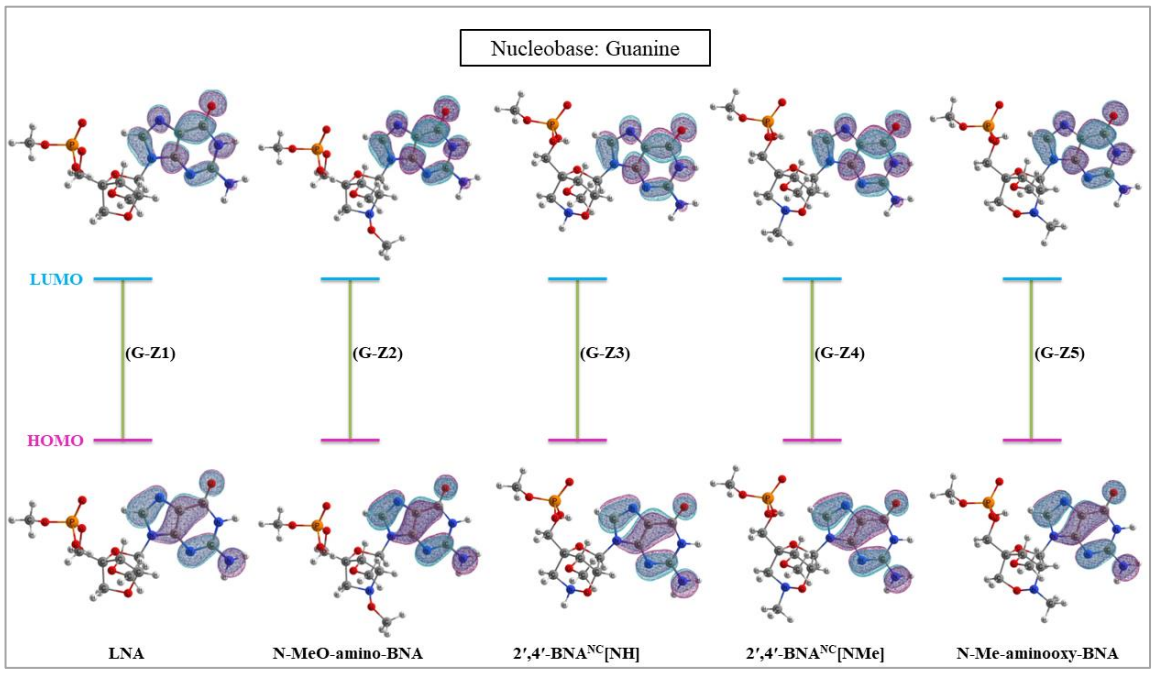
Nucleobase: Guanine
LUMO
HOMO
(G-Z1)
(G-Z2)
(G-Z3)
(G-Z4)
(G-Z5)
LNA
N-MeO-amino-BNA
2′,4′-BNA^NC[NH]
2′,4′-BNA^NC[NMe]
N-Me-aminooxy-BNA

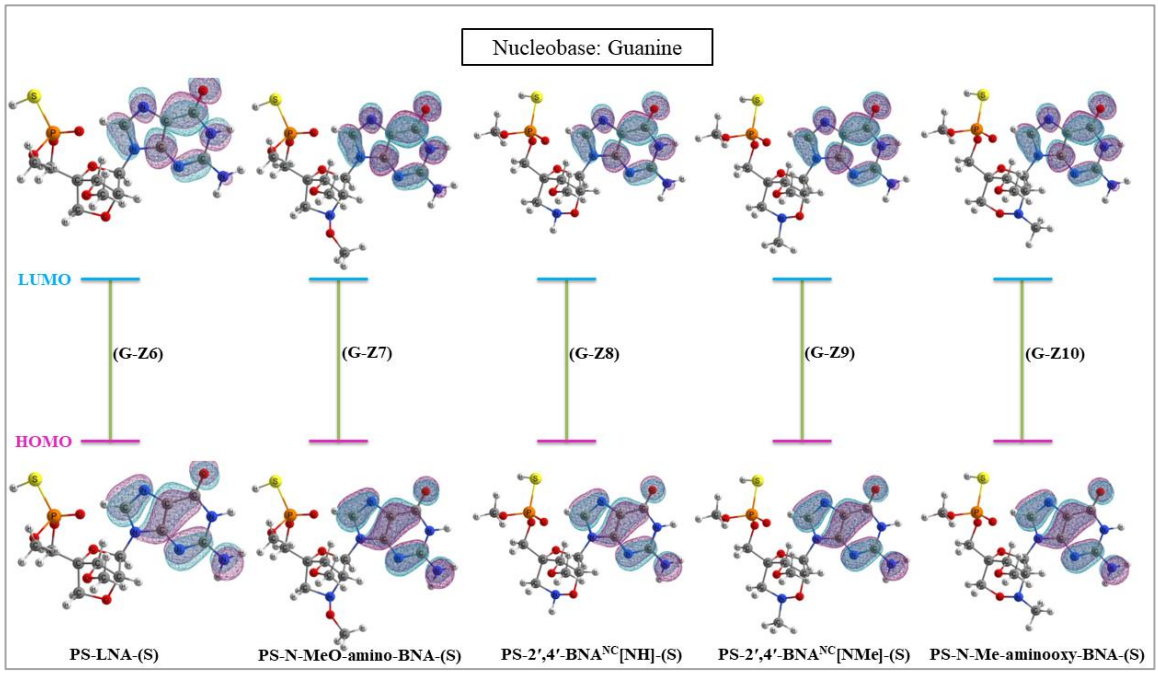
Nucleobase: Guanine
LUMO
HOMO
(G-Z6)
(G-Z7)
(G-Z8)
(G-Z9)
(G-Z10)
PS-LNA-(S)
PS-N-MeO-amino-BNA-(S)
PS-2′,4′-BNA^NC[NH]-(S)
PS-2′,4′-BNA^NC[NMe]-(S)
PS-N-Me-aminooxy-BNA-(S)

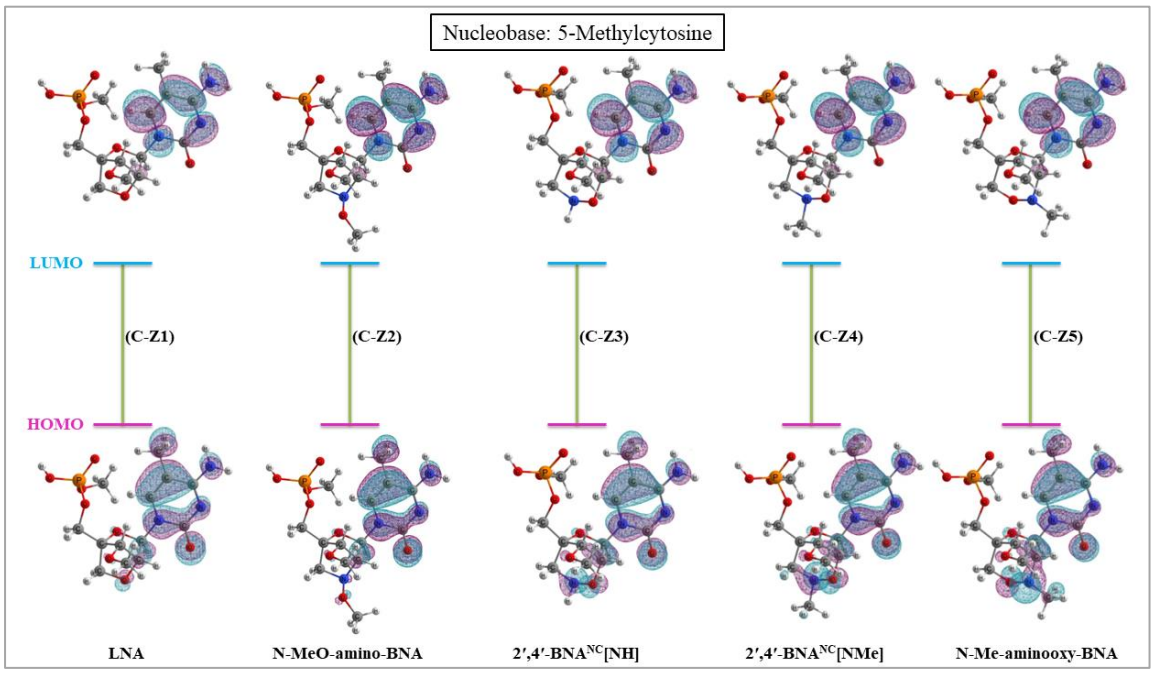
Nucleobase: 5-Methylcytosine
LUMO
HOMO
(C-Z1)
(C-Z2)
(C-Z3)
(C-Z4)
(C-Z5)
LNA
N-MeO-amino-BNA
2′,4′-BNA[NC][NH]
2′,4′-BNA[NC][NMe]
N-Me-aminooxy-BNA

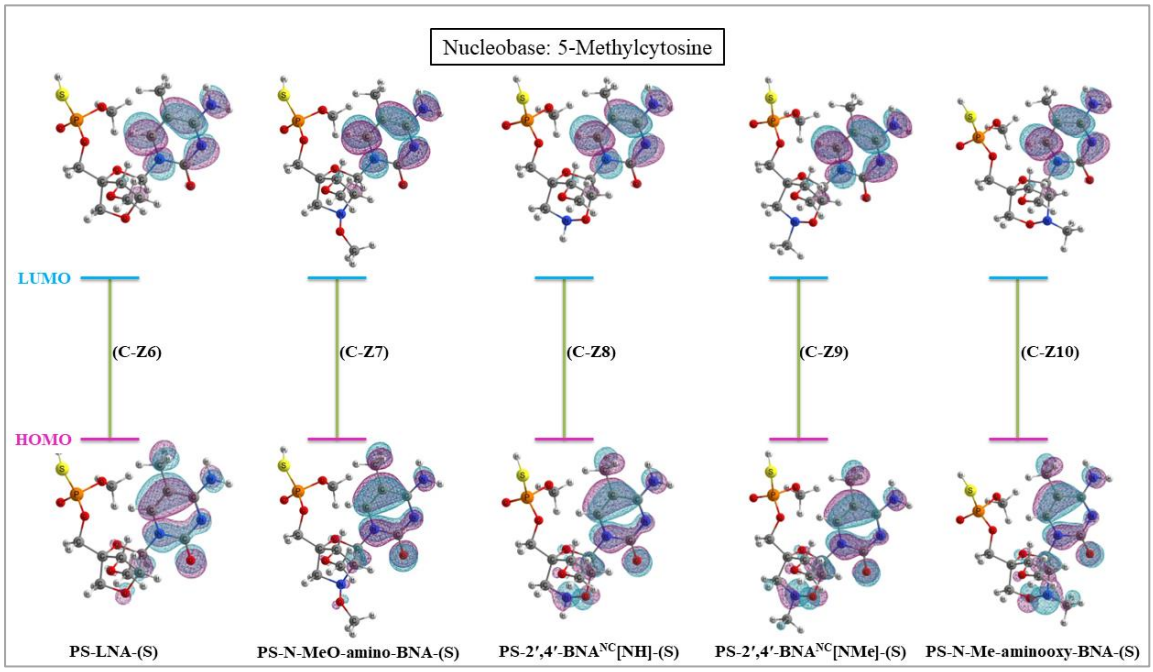
Nucleobase: 5-Methylcytosine
LUMO
HOMO
(C-Z6)
(C-Z7)
(C-Z8)
(C-Z9)
(C-Z10)
PS-LNA-(S)
PS-N-MeO-amino-BNA-(S)
PS-2′,4′-BNA[NC][NH]-(S)
PS-2′,4′-BNA[NC][NMe]-(S)
PS-N-Me-aminooxy-BNA-(S)

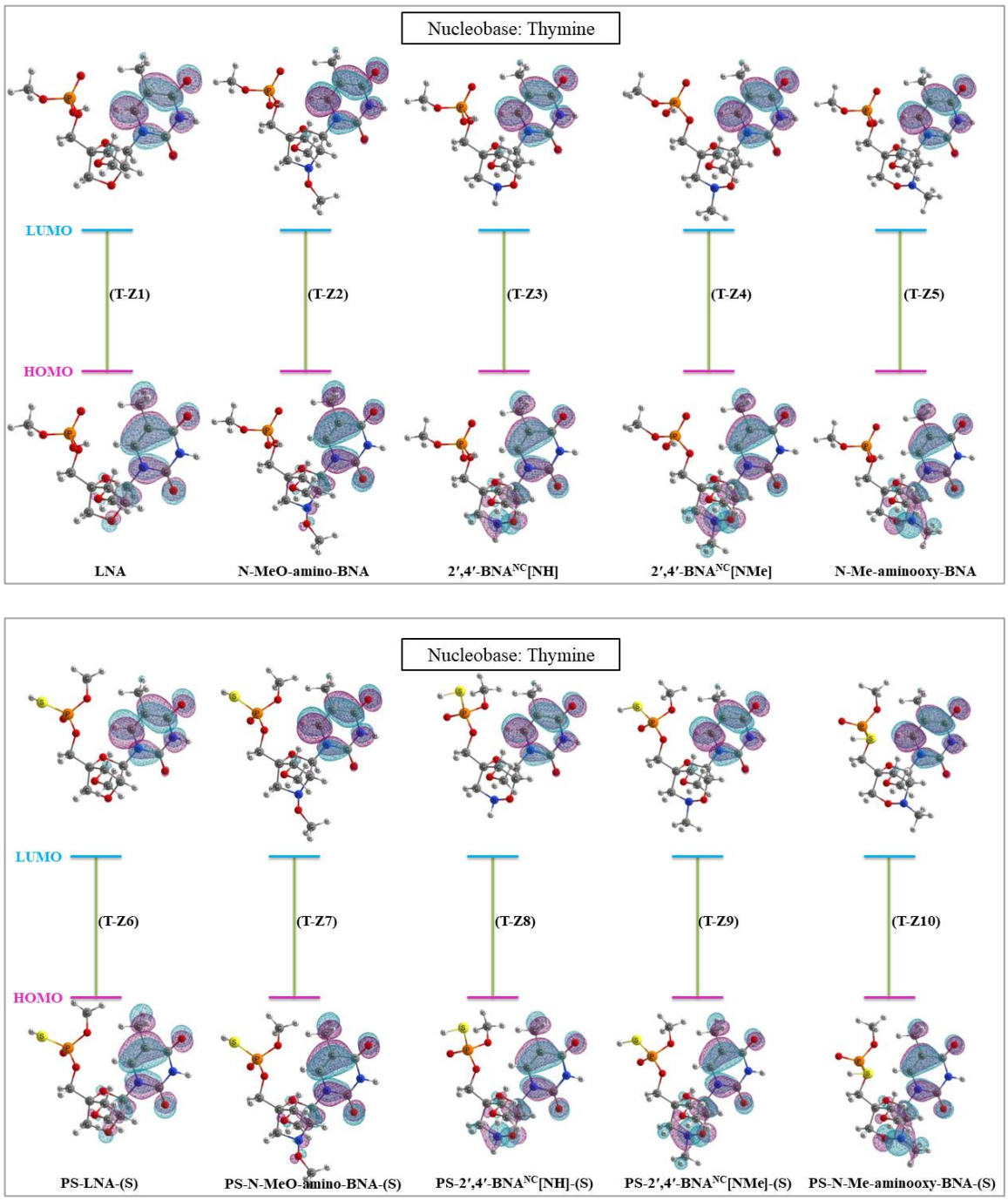

Figure 3.4: HOMO, LUMO iso-surfaces of LNA; N-MeO-amino-BNA; 2′,4′-BNA^{NC}[NH]; 2′,4′-BNA^{NC}[NMe]; N-Me-aminooxy-BNA monomer nucleotides holding normal phosphate backbone (Z1-Z5) and PS-LNA; PS-N-MeO-amino-BNA; PS-2′,4′-BNA^{NC}[NH]; PS-2′,4′-BNA^{NC}[NMe]; PS-N-Me-aminooxy-BNA monomer nucleotides holding phosphorothioate (PS) backbone (Z6-Z10, S-conformers) each containing nucleobase Adenine (A), Guanine (G), 5-Methylcytosine (C) and Thymine (T) calculated at the M06-2X/6-311G(d,p) level of theory.

Natural Bond Orbital (NBO) analysis can be particularly useful in understanding how modifications influence the properties and behavior of modified nucleic acids influence at the molecular level. By analysing the interactions between orbitals, NBO analysis provides information about stabilization energies associated with various electronic effects. This includes hyperconjugation, resonance, charge transfer interactions, determination of bond orders between atoms which contribute to the overall stability of the molecule. This information helps in understanding the strength of bonds within, including hydrogen bonds, covalent bonds, and π-π interactions. The % contributions of each orbital to the HOMO-LUMO were also calculated for the LNA, BNA antisense modifications (Z1-Z5) and for the PS-LNA, PS-BNA antisense modifications (Z6-Z10).

In case of the LNA, BNA antisense modifications (Z1-Z5), it was observed that for all the modifications in adenine nucleobase, the major contributors of the HOMO and LUMO are the 2p orbitals of N(20) and C(15) atoms, respectively. In guanine nucleobase, the major contributors of HOMO and LUMO are the 2p orbital of the C(17) and C(18) atom, respectively. In 5-methylcytosine nucleobase, the major contributors of HOMO and LUMO are the 2p orbital of the C(4) and C(3) atom, respectively. In thymine nucleobase, the major contributors of HOMO and LUMO are the 2p orbital of the C(12) and C(6) atom, respectively. In case of the PS-LNA, PS-BNA antisense modifications (Z6-Z10, S-conformers), it was observed that for all the modifications in adenine nucleobase, the major contributors of the HOMO and LUMO are the 2p orbitals of N(18) and C(13) atoms, respectively. In guanine nucleobase, the major contributors of HOMO and LUMO are the 2p orbital of the C(15) and C(16) atom, respectively. In 5-methylcytosine nucleobase, the major contributors of HOMO and LUMO are the 2p orbital of the C(4) and C(3) atom, respectively. In thymine nucleobase, the major contributors of HOMO and LUMO are the 2p orbital of the C(10) and C(4) atom, respectively. Whether the nucleobase was pyrimidines or purines, the HOMO-LUMO isosurfaces of all the monomer nucleotides were primarily found on the nucleobase area. One of the main factors favouring falloff in their interactions with RNase H may be that they are anchored within. And hence, the non-RNase H activating portion of the duplexes would be less available for different electron-exchange activities during duplex formation with target RNAs. Therefore, instead of designing BNA modifications with MO-isosurfaces positioned in the nucleobase area, one can choose to build BNA modifications with MO-isosurfaces dispersed throughout the modified bridging unit.

3.3.1.3. Global reactivity descriptors of LNA, BNA, PS-LNA, PS-BNA monomer nucleotides

Molecular variations in correlated structures lead to changes in their molecular properties. These properties describe the adjustment of chemical reactivity and stability of a molecule with changing structural configuration of the molecule which can be investigated through the changes in their molecular descriptors. Such studies on quantum chemical parameters have been subjected to various types of small chemical compounds and their derivatives including a few modified nucleobases as well. The present work concentrates on the global reactivity descriptors global hardness (η), global softness (S), chemical potential (μ) and electrophilicity (ω) of the titled LNA, BNA and PS-LNA, PS-BNA monomer nucleotides estimated at the M06-2X/6-311G(d,p) level of theory are shown Figure 3.5, 3.6 and listed in Table 3.4, 3.5 respectively.

Table 3.4: Global hardness (η) Global softness (S) Chemical potential (μ) and Electrophilicity (ω) of LNA; N-MeO-amino-BNA; 2′,4′-BNA^{NC}[NH]; 2′,4′-BNA^{NC}[NMe] and N-Me-aminooxy-BNA monomer nucleotides holding normal phosphate backbone (Z1-Z5) each containing nucleobases Adenine (A), Guanine (G), 5-Methylcytosine (C) and Thymine (T) calculated at the M06-2X/6-311G(d,p) level of theory.

Name Code	Without PS substitution				Name Code	Without PS substitution			
	(η)	(S)	(μ)	(ω)		(η)	(S)	(μ)	(ω)
A-Z1	3.855	0.130	-3.769	1.843	C-Z1	3.835	0.130	-3.879	1.962
A-Z2	3.854	0.130	-3.774	1.848	C-Z2	3.844	0.130	-3.880	1.958
A-Z3	3.852	0.130	-3.757	1.832	C-Z3	3.813	0.131	-3.821	1.915
A-Z4	3.852	0.130	-3.753	1.829	C-Z4	3.804	0.131	-3.814	1.912
A-Z5	3.846	0.130	-3.757	1.835	C-Z5	3.772	0.133	-3.781	1.895
G-Z1	3.944	0.127	-3.400	1.465	T-Z1	3.905	0.128	-4.035	2.085
G-Z2	3.941	0.127	-3.393	1.461	T-Z2	3.915	0.128	-4.032	2.076
G-Z3	3.940	0.127	-3.356	1.429	T-Z3	3.868	0.129	-3.967	2.034
G-Z4	3.940	0.127	-3.356	1.429	T-Z4	3.857	0.130	-3.942	2.014
G-Z5	3.939	0.127	-3.356	1.430	T-Z5	3.810	0.131	-3.913	2.009

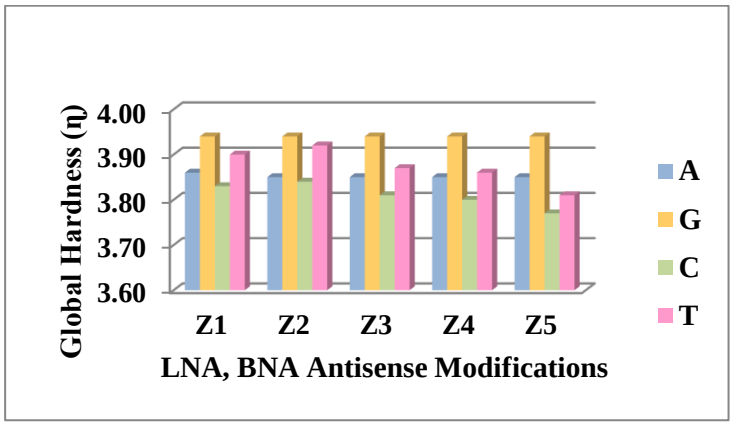
Global Hardness (η)
4.00
3.90
3.80
3.70
3.60
Z1
Z2
Z3
Z4
Z5
LNA, BNA Antisense Modifications
A
G
C
T

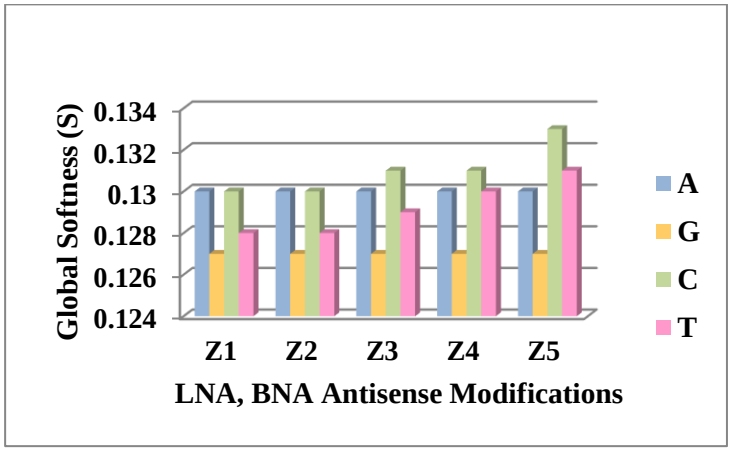
Global Softness (S)
0.134
0.132
0.13
0.128
0.126
0.124
Z1
Z2
Z3
Z4
Z5
LNA, BNA Antisense Modifications
A
G
C
T

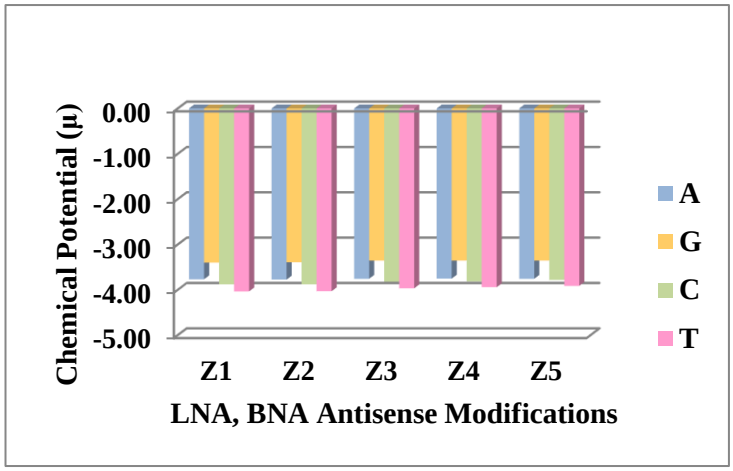
Chemical Potential (μ)
0.00
-1.00
-2.00
-3.00
-4.00
-5.00
Z1
Z2
Z3
Z4
Z5
LNA, BNA Antisense Modifications
A
G
C
T

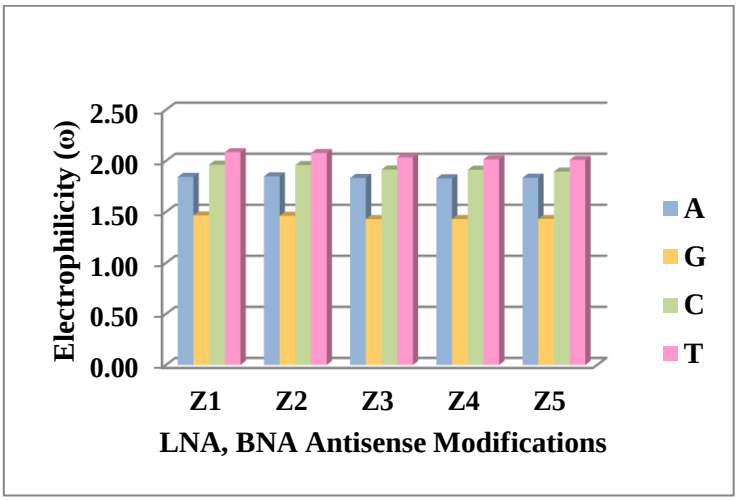

Figure 3.5: Global hardness (η), Global softness (S), Chemical potential (μ) and Electrophilicity (ω) of LNA; N-MeO-amino-BNA; 2′,4′-BNA^{NC}[NH]; 2′,4′-BNA^{NC}[NMe], N-Me-aminooxy-BNA monomer nucleotides holding normal phosphate backbone (Z1-Z5), containing nucleobases Adenine (A), Guanine (G), 5-Methylcytosine (C) and Thymine (T) calculated at the M06-2X/6-311G(d,p) level of theory.

Table 3.5: Global hardness (η), Global softness (S), Chemical potential (μ) and Electrophilicity (ω) of PS-LNA; PS-N-MeO-amino-BNA; PS-2′,4′-BNA^{NC}[NH]; PS-2′,4′-BNA^{NC}[NMe] and PS-N-Me-aminooxy-BNA monomer nucleotides holding phosphorothioate (PS) backbone (Z6-Z10, S conformers) each containing nucleobases Adenine (A), Guanine (G), 5-Methylcytosine (C) and Thymine (T) calculated at the M06-2X/6-311G(d,p) level of theory.

Name Code	S-conformer				Name Code	S-conformer			
	(η)	(S)	(μ)	(ω)		(η)	(S)	(μ)	(ω)
A-Z6	3.858	0.130	-3.788	1.860	C-Z6	3.838	0.130	-3.881	1.963
A-Z7	3.857	0.130	-3.786	1.858	C-Z7	3.848	0.130	-3.876	1.952
A-Z8	3.850	0.130	-3.779	1.855	C-Z8	3.810	0.131	-3.830	1.925
A-Z9	3.849	0.130	-3.786	1.862	C-Z9	3.801	0.132	-3.822	1.922
A-Z10	3.845	0.130	-3.778	1.856	C-Z10	3.771	0.133	-3.787	1.902
G-Z6	3.946	0.127	-3.374	1.442	T-Z6	3.902	0.128	-4.053	2.105
G-Z7	3.943	0.127	-3.367	1.437	T-Z7	3.915	0.128	-4.038	2.082
G-Z8	3.941	0.127	-3.358	1.431	T-Z8	3.864	0.129	-3.960	2.029
G-Z9	3.940	0.127	-3.358	1.431	T-Z9	3.841	0.130	-3.955	2.036
G-Z10	3.939	0.127	-3.357	1.431	T-Z10	3.813	0.131	-3.908	2.003

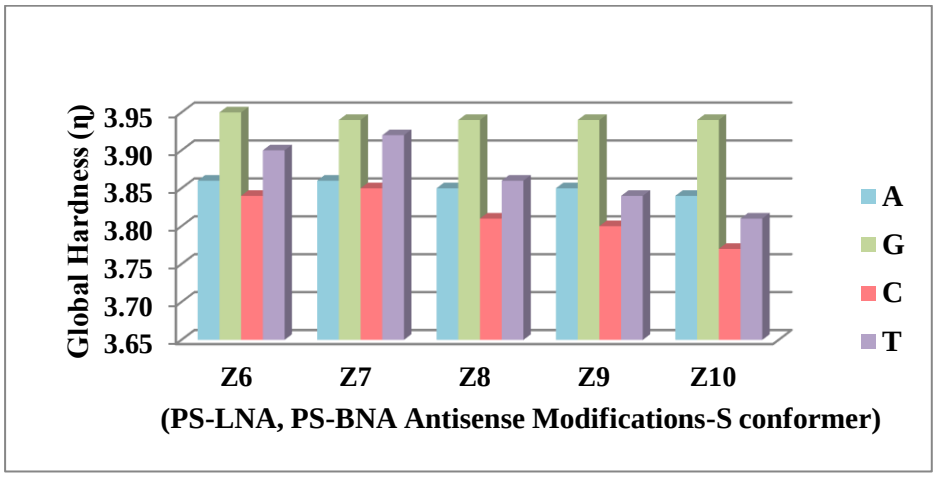
Global Hardness (η)
3.95
3.90
3.85
3.80
3.75
3.70
3.65
Z6
Z7
Z8
Z9
Z10
A
G
C
T
(PS-LNA, PS-BNA Antisense Modifications-S conformer)

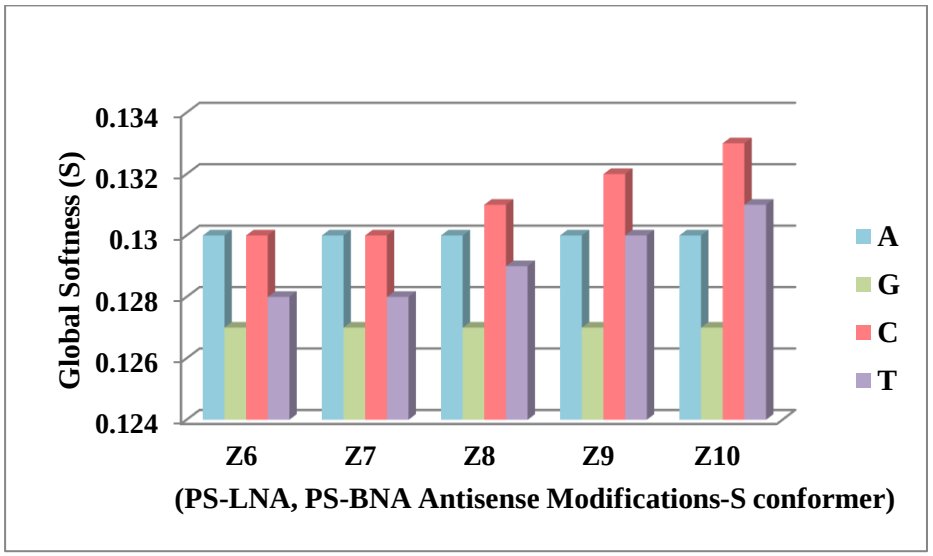
Global Softness (S)
0.134
0.132
0.13
0.128
0.126
0.124
Z6
Z7
Z8
Z9
Z10
A
G
C
T
(PS-LNA, PS-BNA Antisense Modifications-S conformer)

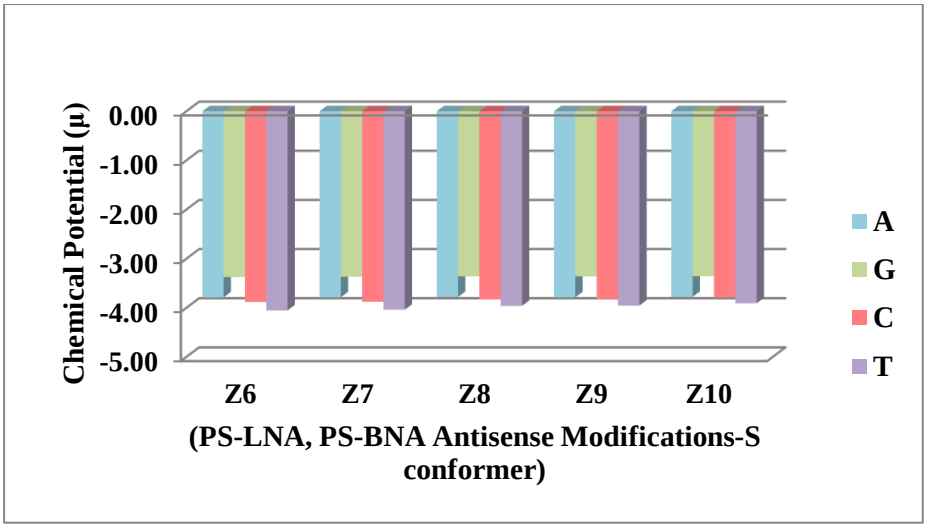
Chemical Potential (μ)
0.00
-1.00
-2.00
-3.00
-4.00
-5.00
Z6
Z7
Z8
Z9
Z10
A
G
C
T
(PS-LNA, PS-BNA Antisense Modifications-S conformer)

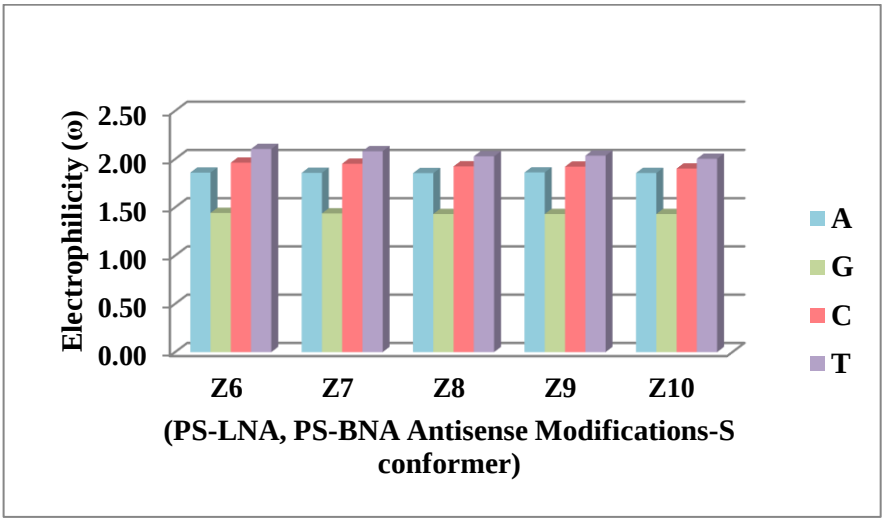

Figure 3.6: Global hardness (η), Global softness (S), Chemical potential (μ) and Electrophilicity (ω) of PS-LNA; PS-N-MeO-amino-BNA; PS-2′,4′-BNA^{NC}[NH]; PS-2′,4′-BNA^{NC}[NMe] and PS-N-Me-aminooxy-BNA monomer nucleotides holding phosphorothioate (PS) backbone (Z6-Z10, S conformers) each containing nucleobases Adenine (A), Guanine (G), 5-Methylcytosine (C) and Thymine (T) calculated at the M06-2X/6-311G(d,p) level of theory.

A detailed study as such on the global reactivity descriptors derived from the HOMO-LUMO energies would provide an in-depth scope to relate the drug like nature of the LNA, BNA, PS-LNA, PS-BNA monomer nucleotides bearing similar molecular structures. Global hardness (η) and global softness (S) provide qualitative evidence of a molecule's polarizability and resistance to deformation, respectively. Molecules with higher values of global hardness do not have easily excitable outer electrons and are less polarizable. It is associated with a larger ΔE_{gap}. On the contrary, associated with a smaller ΔE_{gap}, molecules with higher values of global softness have easily accessible outer electrons and are more polarizable. Thus, hard molecules have larger ΔE_{gap} while soft molecules have smaller ΔE_{Gap}, comparatively. In general, a high ΔE_{Gap} is associated with a more stable chemical state, whereas a lower ΔE_{Gap} is associated with a more reactive state. Results from ΔE_{Gap}, η and S values suggests that the titled antisense modifications over guanine nucleobases will be chemically more stable or less active in electron receiving and elimination processes during a chemical reaction and hence less soft compared to the other nucleobases. On the other hand, particular antisense modifications over nucleobase 5-methylcytosine will be chemically more active in the respective electron receiving and elimination processes and hence softer compared to the other nucleobases.

Other associated parameters like the chemical potential (μ) and electrophilicity (ω) can also be used to determine relative reactivity of the monomer nucleotides. Chemical potential (μ) is the electronic chemical potential that measures an infinitesimal change in energy upon addition of electronic charge. Results from chemical potential values suggests that modifications on thymine nucleobase have more negative chemical potential values and modifications on the guanine nucleobase have less negative chemical potential values irrespective of the type of modifications contained *viz.* the LNA, BNA antisense modifications (Z1-Z5) and the PS-LNA, PS-BNA antisense modifications (Z6-Z10). Electrophilicity (ω) is related to the stabilization of energy when a system gets saturated by electrons from an external environment and serves as an indicator of the reactivity of a system towards nucleophiles and electrophiles. Lower values of ω are an indicative of good nucleophilic character, while higher values of ω are an indicative of a good electrophilic character. Electrophilicity values suggest that modifications on guanine nucleobases are less electrophilic while modifications on the thymine nucleobases are more electrophilic compared to the other nucleobases. This is an implication of guanine nucleobases having high lying E_{HOMO}, high lying E_{LUMO} which will accept electrons less easily, rather will donate more easily and hence less electrophilic. Thymine nucleobases on the other hand having low lying E_{HOMO}, low lying E_{LUMO} will donate electrons less easily, rather will accept more easily and hence more electrophilic. Overall, for both the type of modifications *viz.* the LNA, BNA and the PS-LNA, PS-BNA antisense modifications have less negative chemical potential and are less electrophilic for purine nucleobases over pyrimidine nucleobases.

3.3.2. MD Simulation Results

3.3.2.1. Dynamics of LNA/RNA, BNA/RNA, PS-LNA/RNA, PS-BNA/RNA oligomer duplexes

Exploring the design possibilities of LNA analogues has led to many BNA antisense alterations of being tested for various potential biological activities. However, it is unworthy to develop the analogues without testing their capability to strongly duplex with their targets, especially when it is a natural mRNA. Thus, a set of 14-mer ASO/RNA duplex gapmers, the ASO strand containing the PS-LNA, PS-BNA antisense modifications were considered for a detailed MD simulation study accounting two data sets, each simulated for 1 μs simulation time. Structures of the ASO/RNA duplexes containing the titled PS-LNA, PS-BNA antisense modifications considered for the

simulation study are shown in Figure 3.7. A regular, unmodified DNA/RNA hybrid has been considered as the control system for comparison. As for size of the duplexes, earlier experimental studies have reported in an increased potency of second generation ASOs obtained by reducing the length of the oligomers from 20-mer to 14-mer which exhibited excellent safety profile in human clinical trials [37-39].

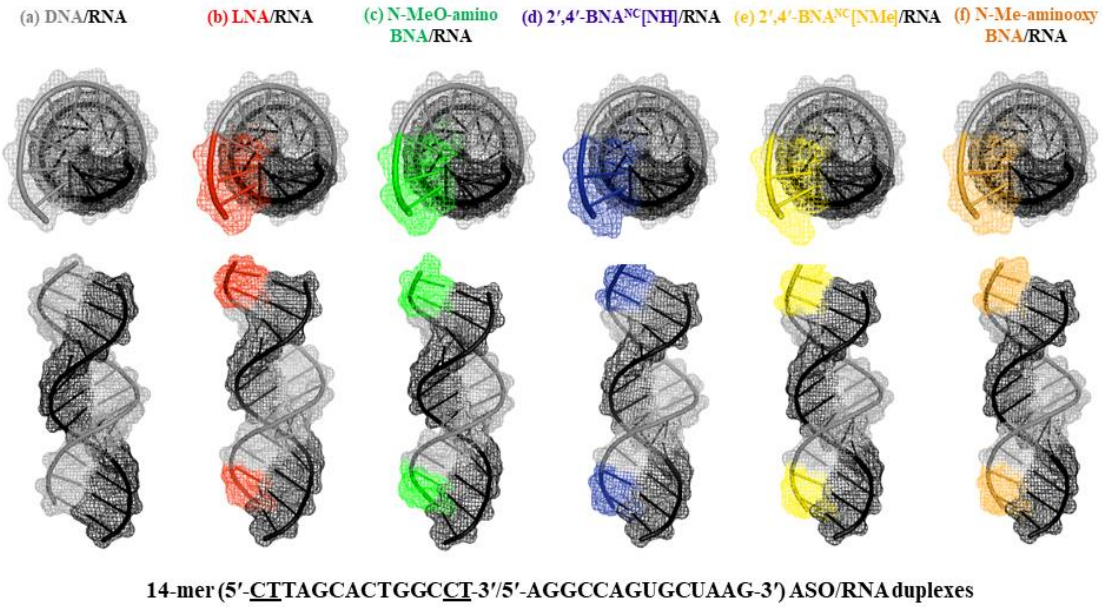

Figure 3.7: Structures of 14-mer ASO/RNA duplexes (a) DNA/RNA (b) PS-LNA/RNA (c) PS-N-MeO-amino-BNA/RNA (d) PS-2′,4′-BNA^{NC}[NH]/RNA (e) PS-2′,4′-BNA^{NC}[NMe]/RNA (f) PS-N-Me-aminooxy-BNA/RNA considered for the MD simulation study.

To understand the structural variation of the duplexes, structures of the duplexes at 100 ns time intervals was observed. It is noteworthy to mention that these duplexes are of 14-mer in length, and ASO/RNA duplexes of this length may be prone to helix opening for certain modifications which may require a larger number (>14) of base-pairs to form stable helical structures. The duplexes were seen maintaining stable base-pairing and base-stacking patterns throughout the simulation trajectory with an exception of helix turning for some duplexes on one end of the duplex however the other end maintaining normal helical structures. End terminals of nucleic acids are more prone to helix opening compared to regions within the interior of the helix where base pairing interactions are more stabilized. Towards the end of a helix, there are unpaired bases. These unpaired bases lack the stabilizing interactions that occur between complementary bases in the double helix structure. This reduced stability can result in weaker hydrogen bonding between the bases, making it easier for the helix to open.

Additionally, the two modifications LNA and N-Me-aminooxy-BNA deviating from the ideal helical structures are interestingly four membered BNA modifications whereas the fairly stable modifications PS-2′,4′-BNA^{NC}[NH], PS-2′,4′-BNA^{NC}[NMe] and PS-N-Me-aminooxy-BNA are five membered BNA modifications. The same parametrization and simulation protocol has been used for all the duplexes and yet of all the five modifications, only two of these modifications were deviating from the ideal helical structure. This is a key finding which describes the supremacy of five membered BNAs being more stable over four membered BNAs for short duplexes of 14-mer length and that duplexes of this length may be prone to helix opening in case of the LNA and N-Me-aminooxy-BNA modifications. Since results from both the sets are similar, we thus believe these structures have the potential to serve as a point of reference for detailed future studies for short duplexes in the field of Bridged Nucleic Acids.

Duplexes PS-2′,4′-BNA^{NC}[NH]/RNA, PS-2′,4′-BNA^{NC}[NMe]/RNA and PS-N-Me-aminooxy-BNA/RNA which are our prime systems of interest were seen maintaining comparatively stable base-pairing, base-stacking and helix turning throughout the simulation trajectory for both the sets of simulations (Set-I & Set-II) and only a few terminal residues were fluctuating from either one side of the end. These structures are reported as end residues in general fluctuate more owing to its positional arrangements of being at the end, of being a sensitive area for helix turning and that we are more interested in comparison of the titled BNA modifications with the LNA modifications, and being from the same family, LNA has been considered for comparison purpose only to understand the structural fluctuations more clearly.

All the six duplexes were found to attempt right-handed postures trying to adopt standard *A-form* helices maintaining stable *Watson-Crick* base-pairing and base-stacking pattern identical to the DNA/RNA control system. The modified 2′C-4′C bridges were positioned at the edge of the minor grooves with no steric barrier for duplex formation thereby reducing conformational flexibility of the ribose and increasing local organization of the sugar-phosphate backbone. Insertion of the BNA monomer nucleotides thus did not change the base-pairing and base-stacking patterns, credits to the *N-glycosidic* dihedral angles being in *anti*-conformation. Overall, the modified ASO/RNA duplexes were right-handed helical with well-defined *Watson-Crick* base-pairing, base-stacking pattern and all of the nucleotides being in *anti*-conformations discussed thoroughly in the following sections.

Stability of the structures obtained from the simulation trajectories were analysed by observing the RMSD plots of the ASO/RNA duplexes for the entire simulation trajectory. The RMSD's were plotted in two different ways considering only the middle core region of the duplex in which the modified terminal residues were omitted are plotted in Figure 3.8. In general, terminal residues exhibit higher deviations owing to its positional arrangements of being at the end. Accordingly, RMSD plots of the duplexes showed higher deviation. Visual inspection of the trajectories shows that the systems were fluctuating in and around a range of ~1 Å to 10 Å of RMSD values. Set-I duplexes (a) DNA/RNA (b) PS-LNA/RNA (c) PS-N-MeO-amino-BNA/RNA (d) PS-2′,4′-BNA^{NC}[NH]/RNA (e) PS-2′,4′-BNA^{NC}[NMe]/RNA (f) PS-N-Me-aminooxy-BNA/RNA showed average RMSDs of 2.56, 8.37, 6.27, 5.31, 5.96, 7.06 Å respectively for the complete duplex and 2.09, 6.50, 4.70, 4.20, 4.96, 5.01 Å respectively for the non-terminal residues. Set-II duplexes (a) DNA/RNA (b) PS-LNA/RNA (c) PS-N-MeO-amino-BNA/RNA (d) PS-2′,4′-BNA^{NC}[NH]/RNA (e) PS-2′,4′-BNA^{NC}[NMe]/RNA (f) PS-N-Me-aminooxy-BNA/RNA showed average RMSDs of 2.08, 7.85, 9.41, 6.50, 4.70, 5.39 Å respectively for the complete duplex and 1.62, 5.39, 7.74, 4.97, 3.47, 4.01 Å respectively for the non-terminal residues. Overall, statistics from both the data sets of simulations predicted that deviation of PS-LNA/RNA and PS-N-MeO-amino-BNA/RNA to be higher than the regular DNA/RNA as well as PS-2′,4′-BNA^{NC}[NH]/RNA PS-2′,4′-BNA^{NC}[NMe]/RNA and PS-N-Me-aminooxy-BNA/RNA duplexes. The noticeable fraying of the PS-LNA/RNA and PS-N-MeO-amino-BNA/RNA duplexes might be due to their higher deviation owing to positional arrangements during simulations. N-MeO-amino-BNAs are LNA analogues with an N-Methoxy-amine group at the 2′-O position. A fairly smaller four membered ring of PS-LNA and PS-N-MeO-amino-BNA compared to PS-2′,4′-BNA^{NC}[NH], PS-2′,4′-BNA^{NC}[NMe] and PS-N-Me-aminooxy-BNA which are otherwise five membered ring modifications might have attributed towards dominating positional adjustments of smaller rings due to strain constriction. Thus, the more flexible 2′C-4′C five membered ring modifications like PS-2′,4′-BNA^{NC}[NH], PS-2′,4′-BNA^{NC}[NMe] and PS-N-Me-aminooxy-BNA without much ring constraints might have contributed towards lower deviations during the simulations. Previously reported simulation studies for 100 ns simulation time on 14-mer gapmer duplexes with LNA and MOE modifications depicted RMSD's of ~2-6 Å for the complete duplex and ~1-3 Å for the non-terminal residues [44,75].

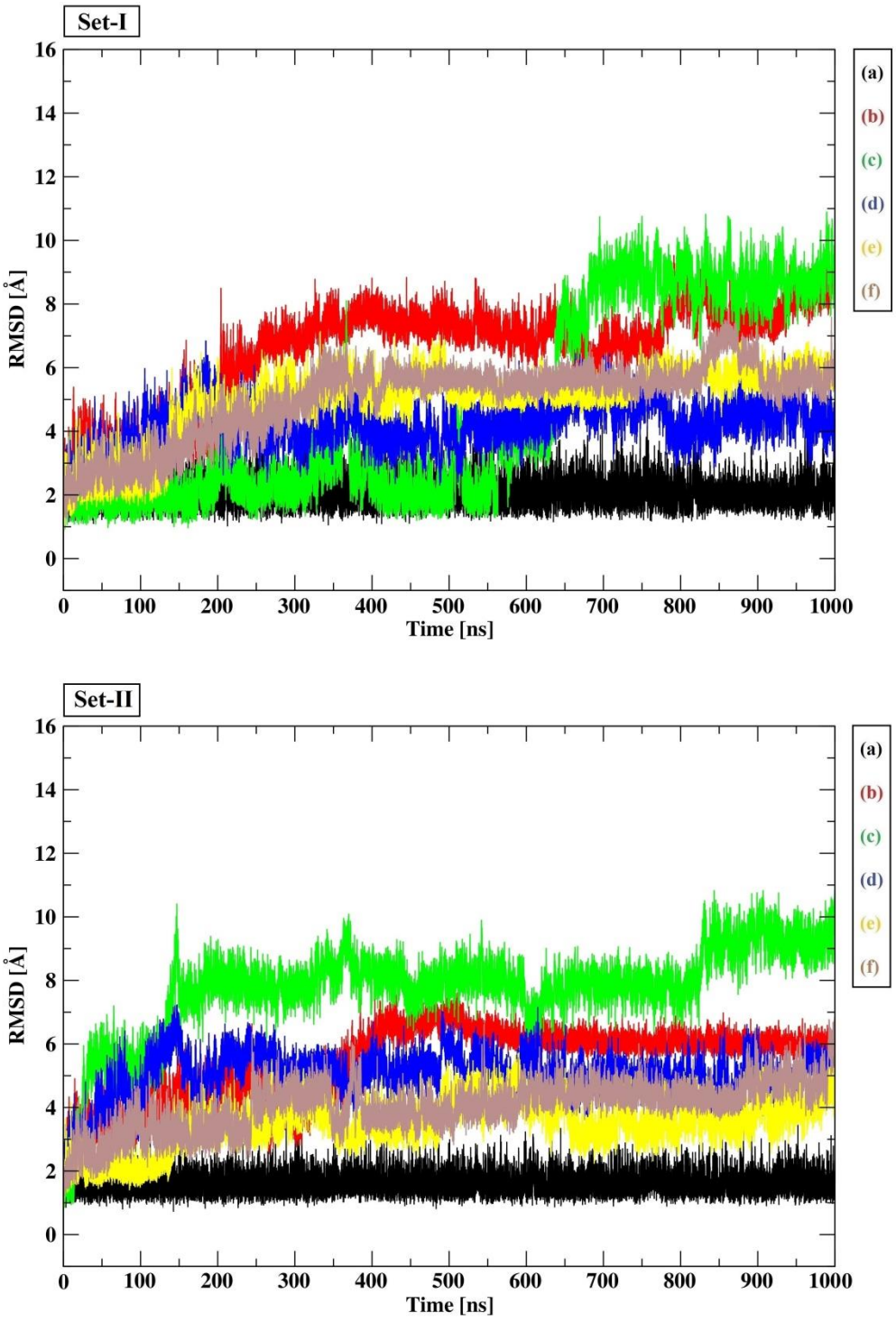

Figure 3.8: RMSD plots of the 14-mer ASO/RNA duplexes (a) DNA/RNA (b) PS-LNA/RNA (c) PS-N-MeO-amino-BNA/RNA (d) PS-2′,4′-BNA^{NC}[NH]/RNA (e) PS-2′,4′-BNA^{NC}[NMe]/RNA and (f) PS-N-Me-aminooxy-BNA/RNA presenting simulation trajectories from two data sets (Set-I & Set-II) each simulated for 1 μs simulation time.

3.3.2.2. Oligomer Duplex Dynamic Structure: Inter-Strand and Intra-Strand PP distances

The molecular double helix of nucleic acid duplexes contains two sugar-phosphate backbones twisted together to form the structural framework of the duplex as a whole. The discussion of inter-strand and intra-strand PP distances in the context of oligomer duplex dynamic structure likely involves analysing the spatial arrangement and flexibility of the phosphate backbone within and between the two strands of the duplex. The term "dynamic structure" indicates that this duplex structure is not static but can undergo changes and fluctuations over time. Herein, higher values of intra-strand phosphate-phosphate (PP) distances (~7 Å) describe *C2'-endo* sugar puckering that can be seen in *B-type* duplexes and lower values of intra-PP distances (~5.9 Å) describe *C3'-endo* sugar puckering that can be seen in *A-type* duplexes [76-77]. Average intra-PP distances of the modified ASO/RNA duplexes for both the strands for the entire simulation trajectory are plotted in Figure 3.9.

In Set-I duplexes, RNA strand residues from the regular DNA/RNA are exhibiting intra-PP distances <6.2 Å which suggest the residues to be in *A-type* conformation and ~6.8 Å for the DNA strand residues which suggest the residues to be in *B-type* conformation. Unlike the RNA strand from the regular DNA/RNA, complementary RNA strands residues from the ASO/RNA duplexes were exhibiting intra-PP distances somewhat higher than the regular RNA strand residues. As for the ASO strands, majority of the non-terminal residues are seen exhibiting lower intra-PP distances compared to the DNA strand residues.

In Set-II duplexes, monomer nucleotides from the regular DNA/RNA are exhibiting intra-PP distances <6.2 Å for the RNA strand residues and ~6.8 Å for the DNA strand residues. Again, the RNA strand from the regular DNA/RNA, RNA strand residues from the ASO/RNA duplexes were exhibiting highly flexible intra-PP distances and nucleotide residues from the ASO strands were showing intra-PP distances lower than the DNA strand residues. Since the modifications are incorporated in the terminal residues, thus the terminal residues were expected to be *A-type* and the non-terminal residues to be *B-type.* However, results from both the data sets revealed that both the strands were trying to compromise with a structure in between an *A-type* and *B-type* conformation.

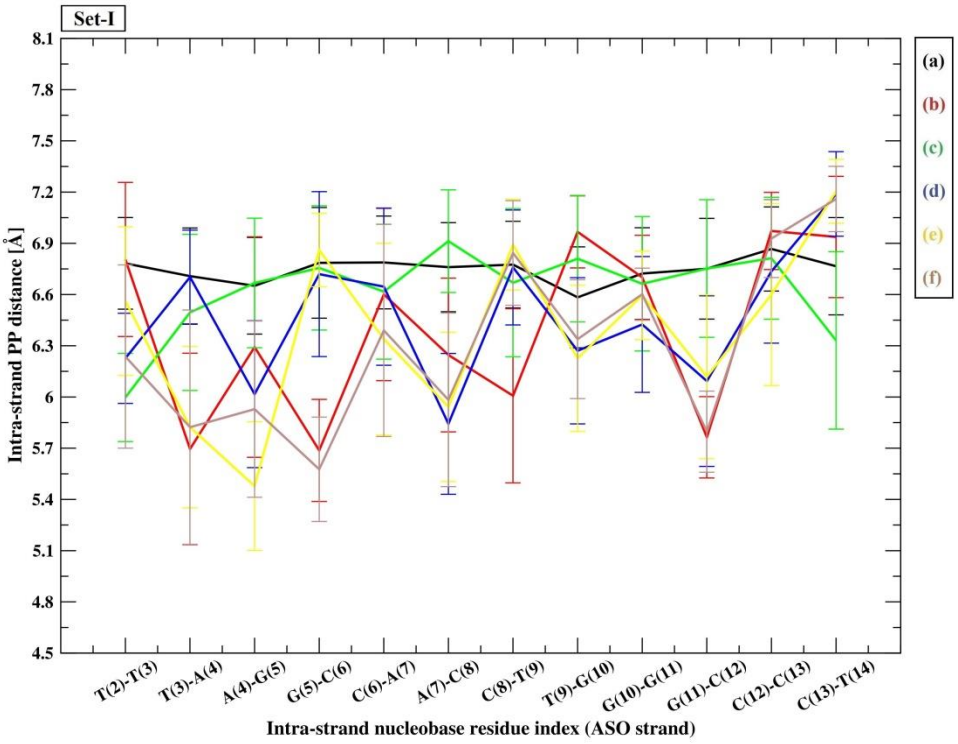
Set-I
Intra-strand PP distance [Å]
8.1
7.8
7.5
7.2
6.9
6.6
6.3
6
5.7
5.4
5.1
4.8
4.5
(a)
(b)
(c)
(d)
(e)
(f)
T(2)-T(3)
T(3)-A(4)
A(4)-G(5)
G(5)-C(6)
C(6)-A(7)
A(7)-C(8)
C(8)-T(9)
T(9)-G(10)
G(10)-G(11)
G(11)-C(12)
C(12)-C(13)
C(13)-T(14)
Intra-strand nucleobase residue index (ASO strand)

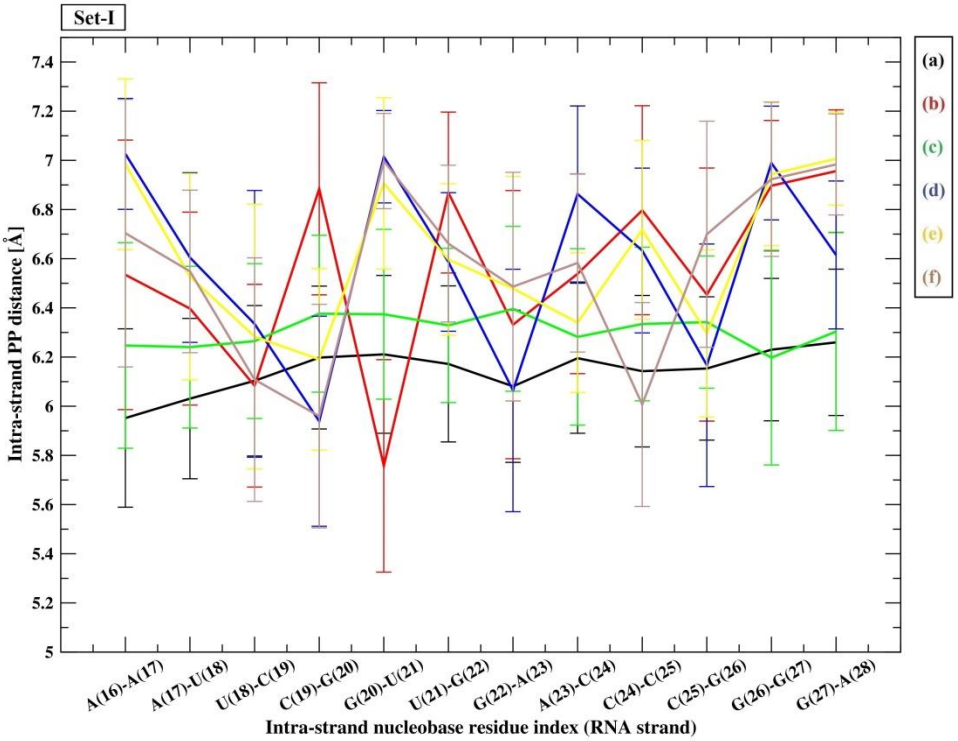
Set-I
Intra-strand PP distance [Å]
7.4
7.2
7
6.8
6.6
6.4
6.2
6
5.8
5.6
5.4
5.2
5
(a)
(b)
(c)
(d)
(e)
(f)
A(16)-A(17)
A(17)-U(18)
U(18)-C(19)
C(19)-G(20)
G(20)-U(21)
U(21)-G(22)
G(22)-A(23)
A(23)-C(24)
C(24)-C(25)
C(25)-G(26)
G(26)-G(27)
G(27)-A(28)
Intra-strand nucleobase residue index (RNA strand)

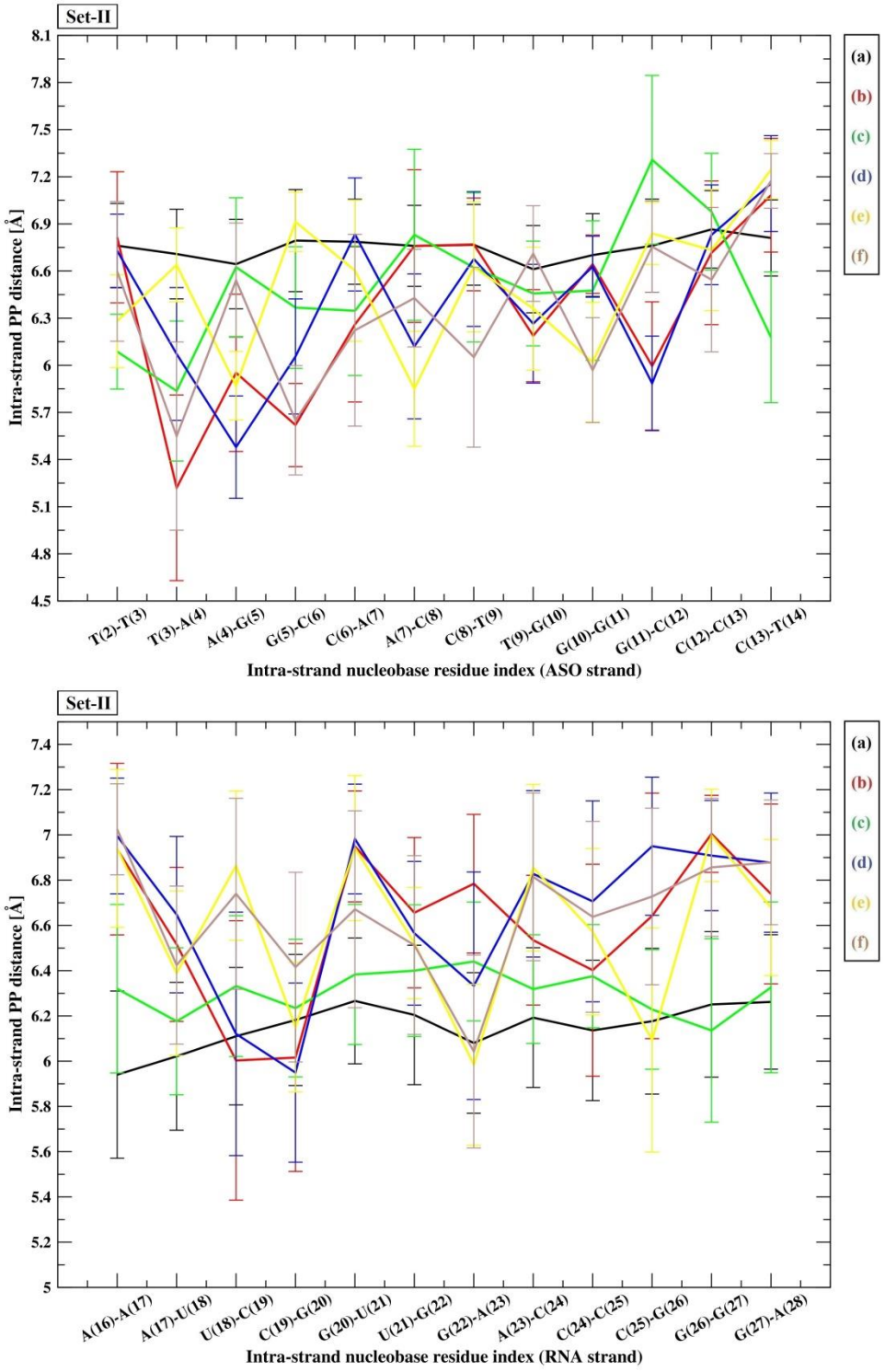

Figure 3.9: Intra-strand PP distances of 14-mer ASO/RNA duplexes (a) DNA/RNA (b) PS-LNA/RNA (c) PS-N-MeO-amino-BNA/RNA (d) PS-2′,4′-BNA^{NC}[NH]/RNA (e) PS-2′,4′-BNA^{NC}[NMe]/RNA and (f) PS-N-Me-aminooxy-BNA/RNA presenting two data sets (Set-I & Set-II) each simulated for 1 μs simulation time.

3.3.2.3. Torsion Angle Dynamics: Sugar-pucker and N-glycosidic torsion angle distribution

"Sugar-pucker" refers to the conformational state of the sugar molecule within a nucleic acid strand. Sugars in nucleic acids can adopt different conformations due to rotation around their bonds wherein the sugar ring adopts a non-planar shape, resembling a puckered or distorted ring. Base-pairing and base-stacking depends on the sugar pucker spectrum of the monomer nucleotides throughout the duplex and accordingly upon the orientation of the phosphate backbone relative to the sugar or the nucleobases. There are pronounced correlations between the sugar-puckering and *N-glycosidic* dihedral angle of the nucleotides which reflect the changes in non-bonded clashes produced by the *C2'-endo* versus *C3'-endo* conformations. Sugar puckers in nucleic acids are either in *C3'-endo* (pucker phase values 0°-40°) or *C2'-endo* (pucker phase values 120°-180°) conformations corresponding to *A-form* or *B-form* conformation in a duplex. Previously, NMR structures including MD simulation studies on LNA ASOs have reported that in an attempt to achieve an overall *A-form* geometry LNA directs a larger population of the sugar puckers into *C3'-endo* conformation. However, the magnitude of such conformational integration in case of the BNA ASOs is less known.

To predict the pucker variations throughout the duplex, sugar puckering distribution of the monomer nucleotides from both the strands of the ASO/RNA duplexes are plotted Figure 3.10. In both Set-1 & Set-II, the regular DNA/RNA is exhibiting *C3'-endo* conformation for RNA strand residues and *C2'-endo* conformation for the DNA strand residues. In the ASO/RNA duplexes, it is expected of the duplex gapmers to maintain a *C2'-endo* conformation by the non-terminal residues for successful recognition by the cellular endonuclease RNase H. Accordingly, both Set-1 & Set-II ASO strand nucleotide monomers were showing a major occupancy of *C3'-endo* conformation for terminal residues and *C2'-endo* conformation for the non-terminal residues. As for the RNA strands, both the terminal and non-terminal residues from the RNA strand were seen to fluctuate in between the *C3'-endo* and the *C2'-endo* conformations. Thus, particular residues from the ASO strands containing the PS-LNA, PS-BNA antisense modifications are clearly visible influencing the sugar puckering pattern on their complementary partner (RNA) strands. This distribution provides insights into the structural flexibility and dynamics of nucleic acids, as well as their interactions with other molecules such as proteins or small ligands.

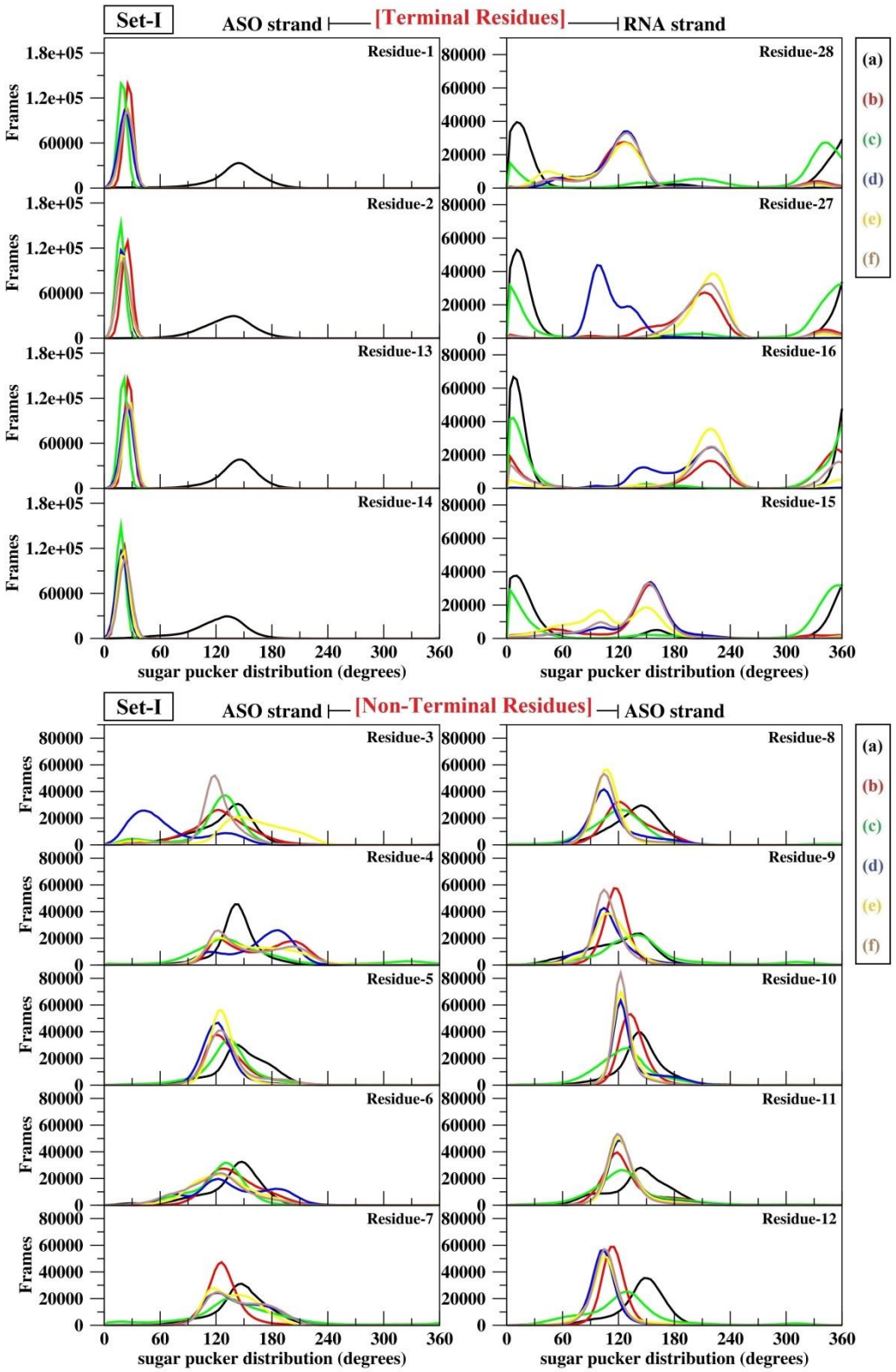
Set-I
ASO strand
[Terminal Residues]
RNA strand
Residue-1
Residue-2
Residue-13
Residue-14
Residue-28
Residue-27
Residue-16
Residue-15
Frames
sugar pucker distribution (degrees)
(a)
(b)
(c)
(d)
(e)
(f)
Set-I
ASO strand
[Non-Terminal Residues]
ASO strand
Residue-3
Residue-4
Residue-5
Residue-6
Residue-7
Residue-8
Residue-9
Residue-10
Residue-11
Residue-12
Frames
sugar pucker distribution (degrees)

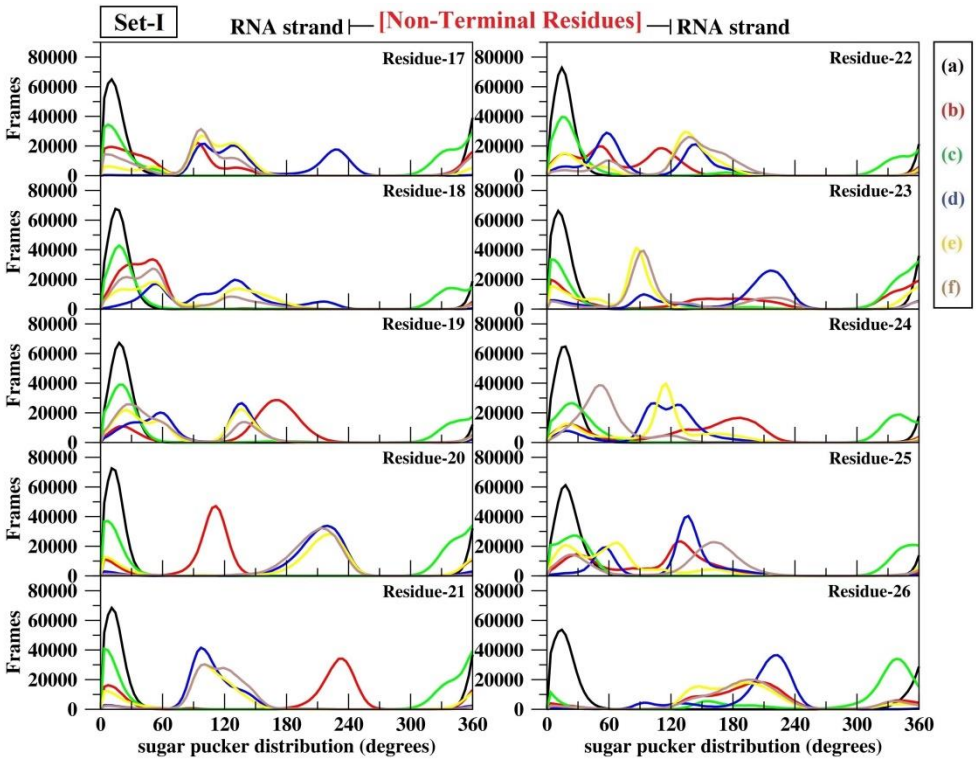
Set-I
RNA strand
[Non-Terminal Residues]
RNA strand
Residue-17
Residue-18
Residue-19
Residue-20
Residue-21
Residue-22
Residue-23
Residue-24
Residue-25
Residue-26
Frames
sugar pucker distribution (degrees)
(a)
(b)
(c)
(d)
(e)
(f)

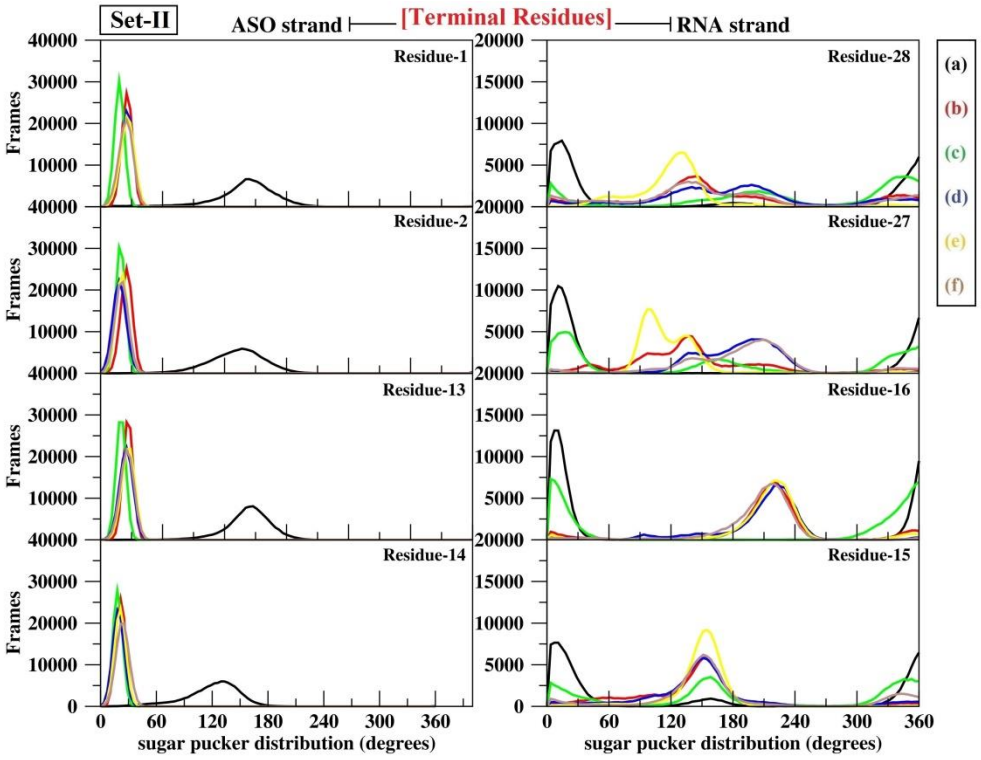
Set-II
ASO strand
[Terminal Residues]
RNA strand
Residue-1
Residue-2
Residue-13
Residue-14
Residue-28
Residue-27
Residue-16
Residue-15
Frames
sugar pucker distribution (degrees)
(a)
(b)
(c)
(d)
(e)
(f)

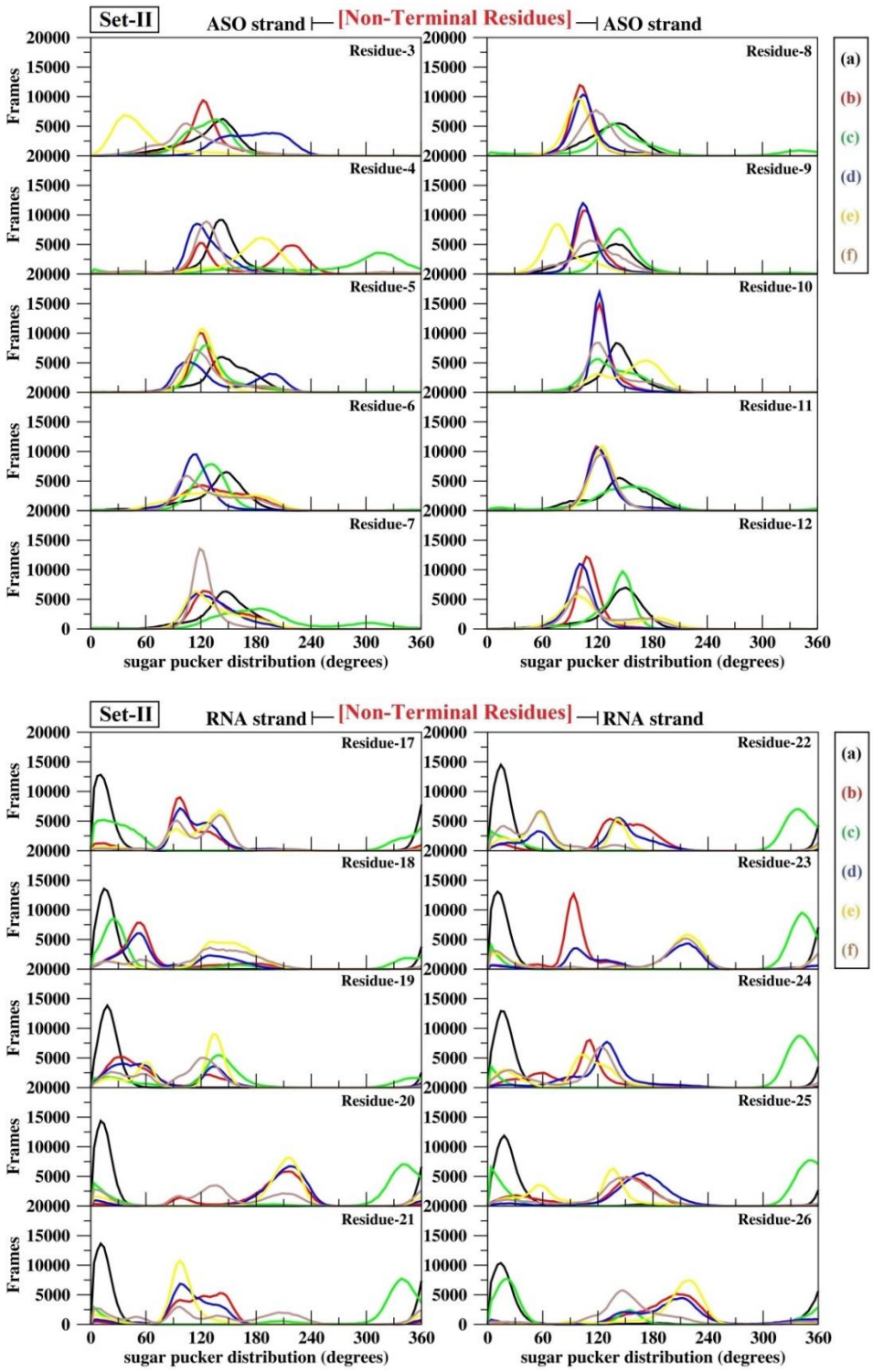

Figure 3.10: Sugar pucker distribution of 14-mer ASO/RNA duplexes (a) DNA/RNA (b) PS-LNA/RNA (c) PS-N-MeO-amino-BNA/RNA (d) PS-2′,4′-BNA^{NC}[NH]/RNA (e) PS-2′,4′-BNA^{NC}[NMe]/RNA (f) PS-N-Me-aminooxy-BNA/RNA presenting two data sets (Set-I & Set-II) each simulated for 1 μs simulation time.

The *N-glycosidic* bond is a measure of the rotation around the bond between the nucleobase and the sugar molecule in a nucleotide. The corresponding *N-glycosidic* dihedral angle chi (χ) describes the orientation of the nucleobase relative to the sugar molecule, specifically the rotation around the bond connecting the nitrogen atom (N) of the nucleobase to the anomeric carbon atom (C1') of the sugar. It is crucial for understanding the spatial arrangement and stacking of bases within the nucleic acid structure. Although chi (χ) can adopt a wide range of values, structural constraints constrict the values for marked preferences. Theory in accordance with experimental findings have predicted two principal low-energy conformations for the *A-form* and *B-form* duplexes wherein χ falls into the ranges of +90° to +180°; –90° to –180° (or 180° to 270°) corresponding to the *anti*-conformation and values in the range of –90° to +90° corresponding to the *syn*-conformation. The *syn* glycosidic angles are not common in nucleotides with *C3'-endo* sugar puckers due to steric confrontation between the nucleobase and the H3′ atom, pointing towards the base in this particular pucker mode.

To explore the rigidity of the nucleotide residues throughout the duplex, *N-glycosidic* torsion distribution of the monomer nucleotides from both the strands of the ASO/RNA duplexes are plotted Figure 3.11. In both Set-1 & Set-II, the regular DNA/RNA is exhibiting chi (χ) values ranging from -90° to -180° for the DNA strand residues and values ranging from -120° to -180° for the RNA strand residues. Both the purines adenine and guanine usually prefer *anti*-conformation in either *A-form* or *B-form* of standard nucleic acid duplexes and pyrimidines always prefer *anti*-conformation even in *Z-form* nucleic acid duplexes. In case of the ASO/RNA duplexes, both Set-1 & Set-II ASO strands were showing a major occupancy of -120° to -180° for the terminal residues and major occupancy of -60° to -180° for non-terminal residues. As for the RNA strands, terminal residues were fluctuating with chi (χ) values ranging between -60° to -180° and the non-terminal residues were fluctuating with values ranging between -120° to -180°. Hence, the residues were trying to maintain their relative sugar-base orientations to be in *anti*-conformation maintaining stable *Watson-Crick* base pairing throughout the duplex for the entire simulation time. The sugar-pucker and *N-glycosidic* torsion angle distribution describe the range of conformations adopted by the sugar molecules and nucleobases within nucleic acid structures. These structural parameters play critical roles in determining the overall shape, stability, and functionality of DNA and RNA molecules in biological systems.

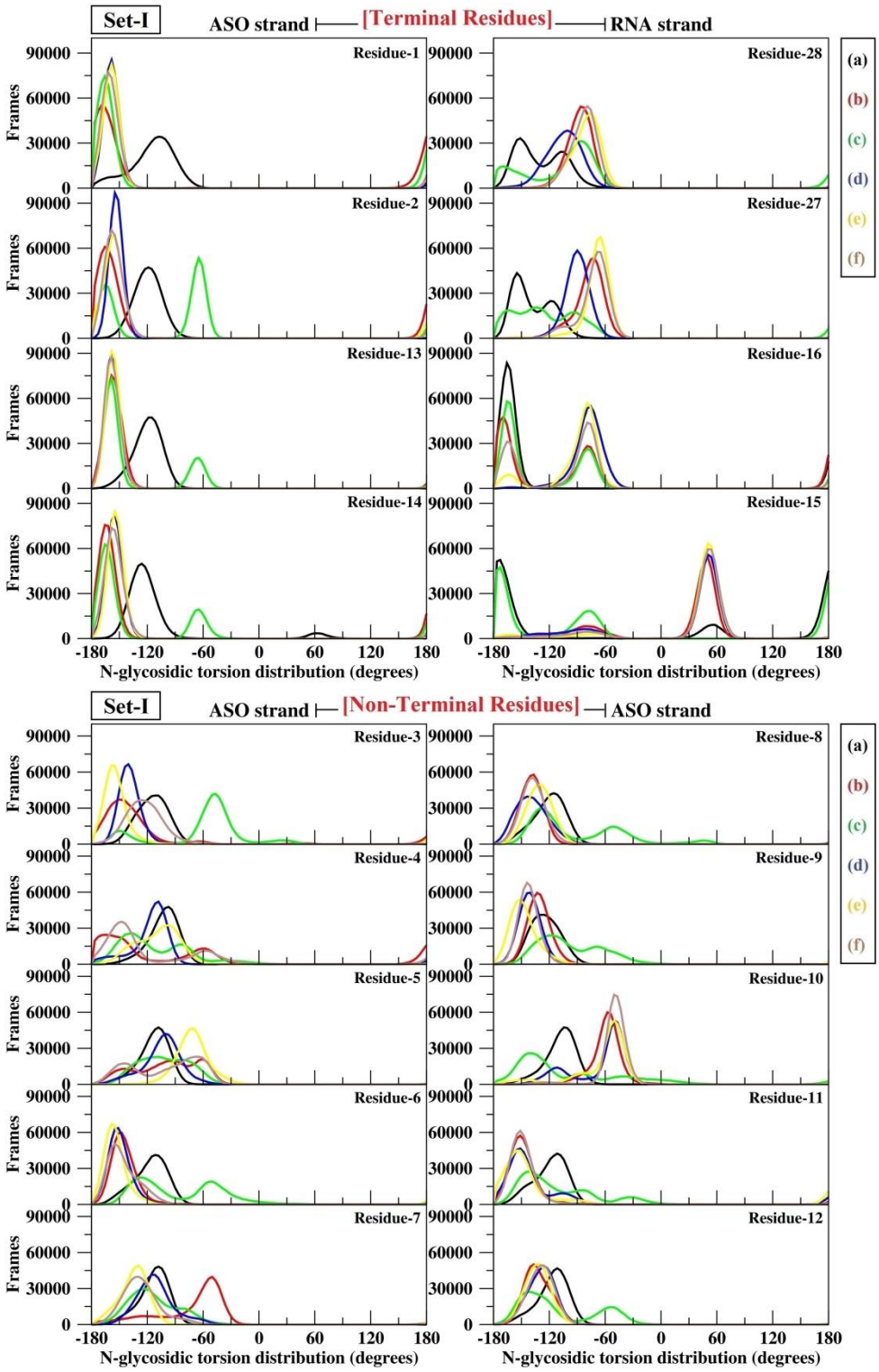
Set-I
ASO strand
[Terminal Residues]
RNA strand
Residue-1
Residue-28
Residue-2
Residue-27
Residue-13
Residue-16
Residue-14
Residue-15
Frames
90000
60000
30000
0
-180
-120
-60
0
60
120
180
N-glycosidic torsion distribution (degrees)
(a)
(b)
(c)
(d)
(e)
(f)
Set-I
ASO strand
[Non-Terminal Residues]
ASO strand
Residue-3
Residue-8
Residue-4
Residue-9
Residue-5
Residue-10
Residue-6
Residue-11
Residue-7
Residue-12

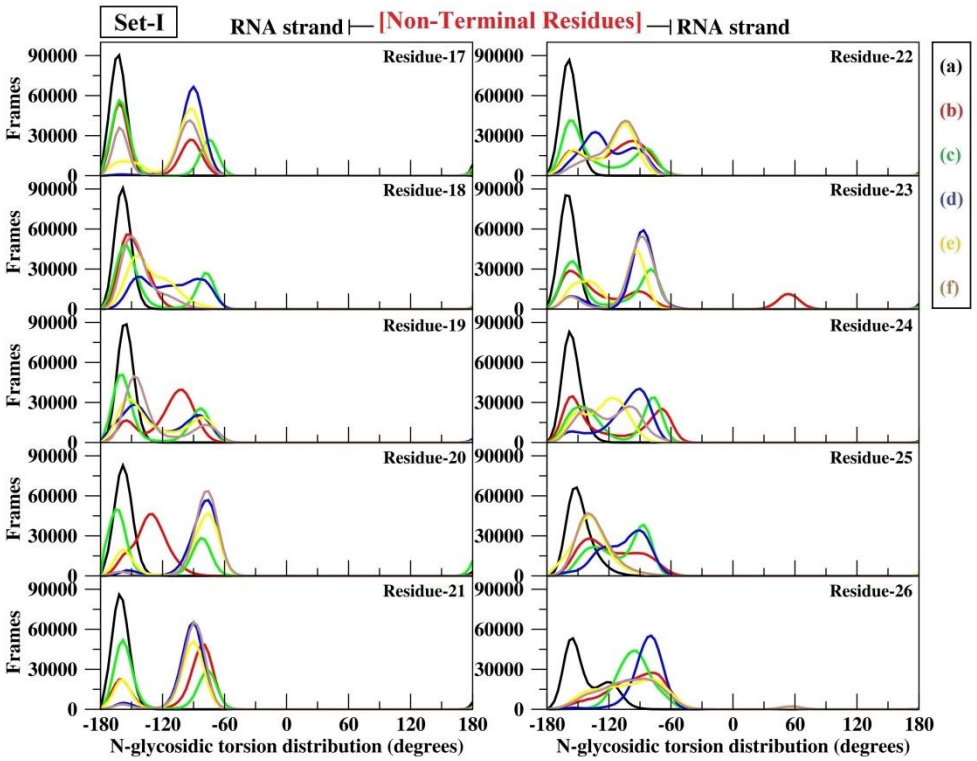
Set-I
RNA strand
[Non-Terminal Residues]
RNA strand
Residue-17
Residue-18
Residue-19
Residue-20
Residue-21
Residue-22
Residue-23
Residue-24
Residue-25
Residue-26
Frames
90000
60000
30000
0
-180
-120
-60
0
60
120
180
N-glycosidic torsion distribution (degrees)
(a)
(b)
(c)
(d)
(e)
(f)

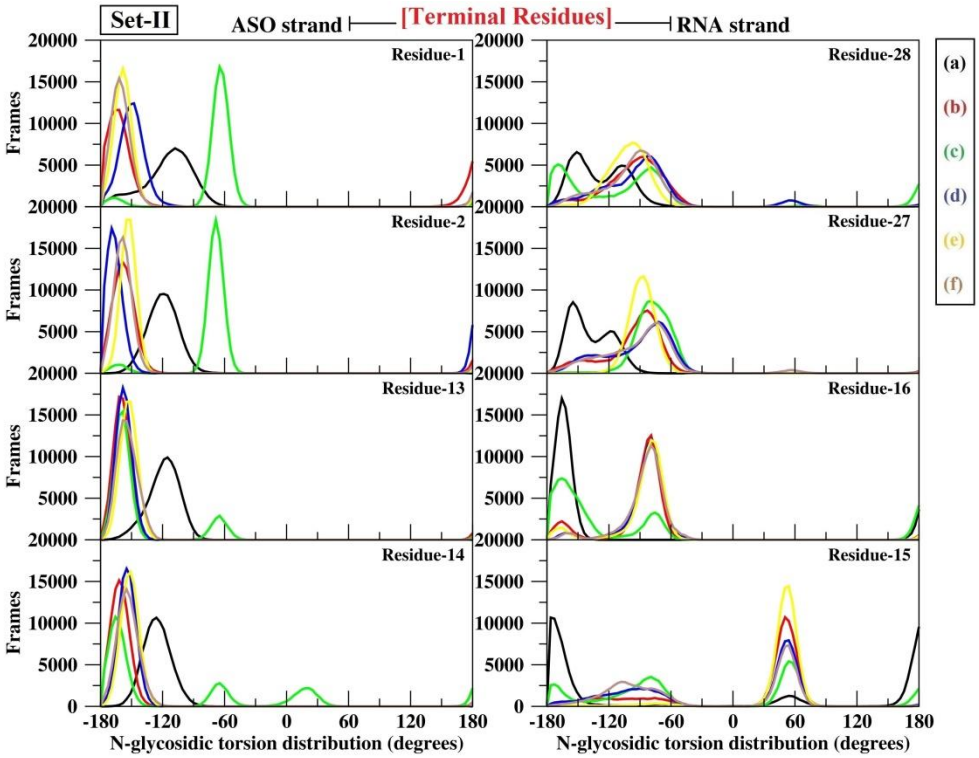
Set-II
ASO strand
[Terminal Residues]
RNA strand
Residue-1
Residue-2
Residue-13
Residue-14
Residue-28
Residue-27
Residue-16
Residue-15
Frames
20000
15000
10000
5000
0
-180
-120
-60
0
60
120
180
N-glycosidic torsion distribution (degrees)
(a)
(b)
(c)
(d)
(e)
(f)

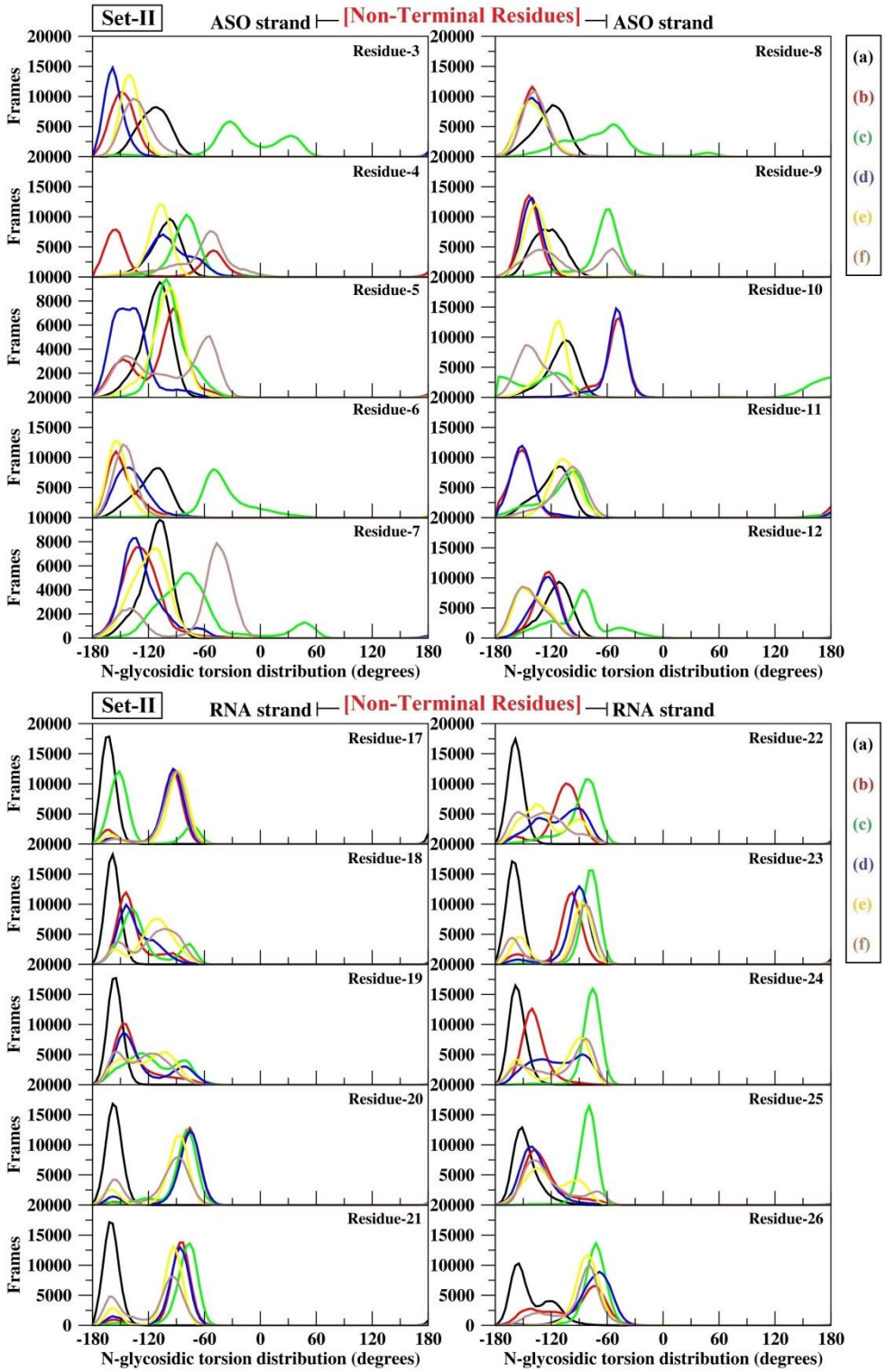

Figure 3.11: N-glycosidic torsion distribution of 14-mer ASO/RNA duplexes (a) DNA/RNA (b) PS-LNA/RNA (c) PS-N-MeO-amino-BNA/RNA (d) PS-2′,4′-BNA^{NC}[NH]/RNA (e) PS-2′,4′-BNA^{NC}[NMe]/RNA (f) PS-N-Me-aminooxy-BNA/RNA presenting two data sets (Set-I & Set-II) each simulated for 1 μs simulation time.

3.3.2.4. Backbone flexibility, Base-pairing and H-Bond interactions

The backbone of DNA and RNA refers to the sugar-phosphate backbone, which forms the structural framework of the molecule. This backbone is flexible, allowing the molecule to adopt various conformations and facilitating processes such as replication, transcription, and protein binding. Backbone flexibility is crucial for the overall conformational dynamics of DNA and RNA, enabling them to undergo structural changes during processes like DNA replication and RNA folding. Sugar-phosphate backbone of nucleic acid duplexes provides directionality and flexibility to the monomer nucleotides throughout the duplex which in-turn plays a major role on imparting superior antisense activity. The active site of the cellular endonuclease RNase H comprises of an RNA-binding groove and a spatially conserved phosphate-binding pocket which defines a DNA-binding channel. Specific binding of DNA/RNA duplexes at the active site of RNase H is highly dependent on the surface complementarity and close fitting of the DNA backbone, making *van der Waals* and H-bond interactions at the active site of RNase H [78]. For successful substrate-binding and cleavage specificity, phosphate at the active site of the RNase H phosphate-binding pocket also requires large distortions of the backbone torsion angles from their ideal values. Depending on the flexibility of the sugar-phosphate backbone, the minor groove width of the DNA/RNA duplexes changes at the phosphate binding pocket of the DNA-binding channel.

To observe the influence of rigid sugar conformations residue wise RMSF of the backbone heavy atoms of the nucleotide residues from both the nucleic acid strands are plotted in Figure 3.12. In general, nucleic acid duplexes, terminal residues exhibit more fluctuations compared to the non-terminal residues. Accordingly, RMSF plots revealed that the terminal residues for both the RNA as well as the DNA strand exhibited higher fluctuations compared to the non-terminal residues. Monomer nucleotides from Set-I ASO/RNA duplexes were seen to exhibit higher backbone flexibility compared to the monomer nucleotides from Set-II ASO/RNA duplexes. Previous studies on fully modified LNA duplexes suggested low backbone flexibility and that the LNA ASOs do not impose its flexibility onto its complementary partner strands. However, flexibility pattern of the LNA/RNA and BNA/RNA duplexes are similar as the DNA/RNA for both Set-I & Set-II. This flexibility has been achieved with due consideration of chimeric gapmers which are rather better choices over fully modified LNA constructs to obtain maximum antisense activity.

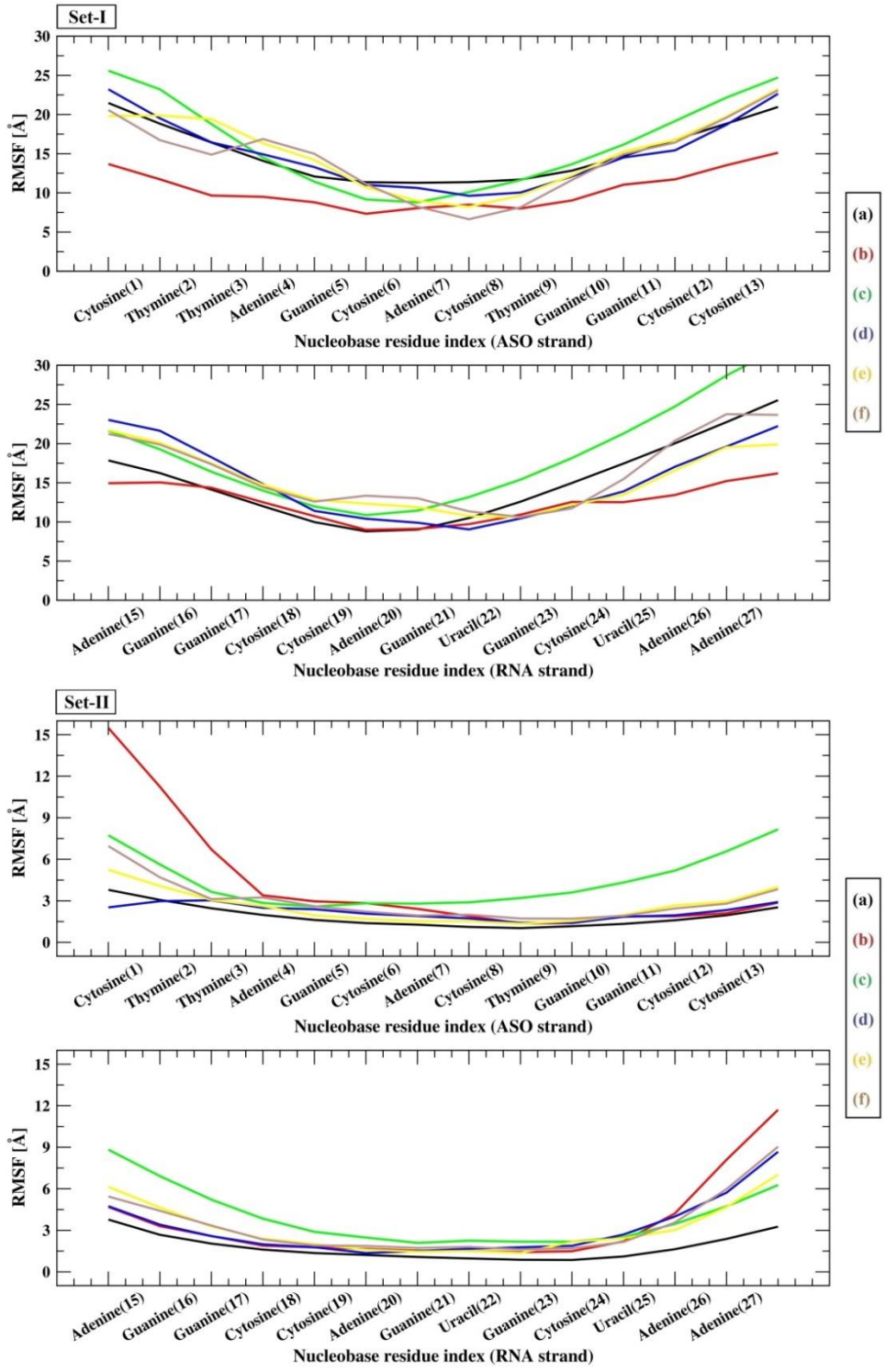

Figure 3.12: RMSF plot of 14-mer ASO/RNA duplexes (a) DNA/RNA (b) PS-LNA/RNA (c) PS-N-MeO-amino-BNA/RNA (d) PS-2′,4′-BNA^{NC}[NH]/RNA (e) PS-2′,4′-BNA^{NC}[NMe]/RNA (f) PS-N-Me-aminooxy-BNA/RNA for both the strands, presenting two data sets (Set-I & Set-II) each simulated for 1 µs simulation time.

Active base pairing is absolutely necessary for RNA functioning because it greatly stabilizes the folded structure of the RNAs, which utilizes the 2′-OH group of the ribose sugar ring [79-80]. Thus, base pairing interactions in the modified ASO/RNA duplexes are of fundamental biological importance for homologous recognition between the two complementary strands of the duplexes which will be impacted by the 2′-oxygen modification of the PS-LNA, PS-BNA antisense modifications. Monomer nucleotides of the ASO/RNA duplexes should exist in an *anti*-conformation to effectively couple with the RNA nucleobases and bind sequence precisely to their target RNAs, a characteristic feature of *A-form* helix typically observed in RNAs [81]. Additionally, the modified nucleobases in complex with the RNA nucleobases should induce the flanking RNAs to adopt or maintain an *N-type* conformation that favors the *C3'-endo* sugar puckering. This will decrease the ribose sugar's conformational flexibility and increase local organization of the phosphate backbone.

Hydrogen bonds play a crucial role in stabilizing the base-pairing interactions in DNA and RNA. These hydrogen bonds are relatively weak individually but collectively provide significant stability to the double helix structure of DNA and RNA. Additionally, hydrogen bonds between the phosphate backbone and water molecules contribute to the solvation and stability of the nucleic acid molecule in an aqueous environment. The base-pairs exhibited inter-strand H-Bond distances of ~2.7-2.9 Å maintaining stable *Watson-Crick* base pairing and H-Bond parameters in agreement with reported values corresponding to the *A*-form duplex structure of RNAs [82]. Both native and non-native contacts between amino acid residues are important in determining the mechanism of proteins folding and unfolding. The interstrand native contacts of *WC* base-pairs of the ASO/RNA duplexes, except for the PS-LNA and PS-N-MeO-amino-BNA/RNA were exhibiting similar contacts as the DNA/RNA control system. the backbone flexibility, base-pairing, and hydrogen bonding interactions are essential features of DNA and RNA that collectively contribute to their structure, stability, and functionality. Understanding these aspects is crucial for unravelling the mechanisms underlying genetic processes and molecular interactions in biology.

3.3.2.5. SASA, MM-GBSA Binding Free Energy of the modified ASO/RNA duplexes

Solvent accessible surface area (SASA) and MM-GBSA binding free energy have long been regarded as a key variable in research on protein folding and drug-protein

stability. Consequently, understanding the solvation functionality and stability of the modified ASO/RNA duplexes can also be benefited from studying the SASA and MM-GBSA free energy of the ASO/RNA duplexes [83]. Thus, solvation pattern of all the ASO/RNA duplexes were evaluated by calculating their SASA values considering the entire simulation trajectory enlisted in Table 3.6. Based on SASA values, nucleotides residues of a duplex can be classified as buried or exposed. The more is the SASA values, the more will be the contact area of the duplexes with the water molecules resulting in increased aqueous solubility of the duplexes. Accordingly, results of SASA values revealed that solvation of all the modified ASO/RNA duplexes for the particular nucleic acid sequence were higher than the DNA/RNA control system for both Set-I & Set-II simulation trajectories.

Table 3.6: SASA and MM-GBSA free energies of 14-mer ASO/RNA duplexes (a) DNA/RNA (b) PS-LNA/RNA (c) PS-N-MeO-amino-BNA/RNA (d) PS-2′,4′-BNA^{NC}[NH]/RNA (e) PS-2′,4′-BNA^{NC}[NMe]/RNA (f) PS-N-Me-aminooxy-BNA/RNA presenting two data sets (Set-I & Set-II) each simulated for 1 μs simulation time.

Set-I	SASA (Å^2)	MM-GBSA (kcal/mol)			
		$G_{ASO/RNA}$	G_{RNA}	G_{ASO}	ΔG
(a) DNA/RNA	5142.46	-3937.35	-2063.55	-1762.14	-111.66
(b) PS-LNA/RNA	5547.60	-6558.36	-3714.00	-2780.39	-63.97
(c) PS-N-MeO-amino-BNA/RNA	5677.96	-3771.69	-2108.85	-1562.35	-100.49
(d) PS-2′,4′-BNA^{NC}[NH] /RNA	5435.81	-3952.34	-2100.83	-1765.77	-85.74
(e) PS-2′,4′-BNA^{NC}[NMe] /RNA	5298.85	-3821.23	-2097.85	-1660.42	-62.96
(f) PS-N-Me-aminooxy-BNA/RNA	5526.13	-3802.77	-2089.49	-1638.64	-74.64
Set-II	**SASA (Å^2)**	**MM-GBSA (kcal/mol)**			
		$G_{ASO/RNA}$	G_{RNA}	G_{ASO}	ΔG
(a) DNA/RNA	5155.81	-3938.65	-2063.30	-1764.27	-111.08
(b) PS-LNA/RNA	5347.19	-3731.41	-2098.64	-1561.70	-71.07
(c) PS-N-MeO-amino-BNA/RNA	5521.43	-3749.99	-2083.33	-1560.44	-106.22
(d) PS-2′,4′-BNA^{NC}[NH] /RNA	5487.95	-3909.09	-2091.65	-1755.56	-61.88
(e) PS-2′,4′-BNA^{NC}[NMe] /RNA	5539.02	-3858.92	-2101.88	-1673.64	-83.40
(f) PS-N-Me-aminooxy-BNA/RNA	5617.18	-3826.24	-2086.59	-1648.52	-91.13

MM-GBSA binding free energy values of all the duplexes for the entire simulation trajectory were also calculated, computed with the equation:

$$\Delta G_{Binding} = G_{ASO/RNA} - G_{ASO} - G_{RNA}$$

Herein, the energies were calculated by considering the RNA strand as the target receptor, the ASO strand as the binding ligand and the ASO/RNA duplexes as the receptor-ligand complex. The average MM-GBSA binding free energy values for the entire trajectory are listed in Table 3.6. For all the duplexes, free energy of the RNA strand has nearly identical energy values. On the other hand, the energy values of the modified ASO strand varied depending on the alterations. LNAs are proven to have enhanced thermodynamic stability, nucleic acid recognition, superior hybridizing affinity, sequence selectivity and improved bio-stability compared to that of natural oligonucleotides. However, for the titled PS-LNA, PS-BNA antisense modifications and for the particular sequence considered binding energies of the modified ASO/RNA duplexes were comparatively lower than the DNA/RNA control system for both Set-I & Set-II simulation trajectories. Solvation of the duplexes although were higher compared to the natural oligonucleotides, their binding energies being relatively lower may lead to decreased antisense activity. Thus, with the various advantageous properties of BNAs over LNAs there is still need to further modify these BNA antisense modifications.

3.4. Summary

The primary goal of the present work was to perform a detailed quantum chemical study of a few LNA, BNA and PS modified LNA, BNA antisense modifications at the monomer level using DFT methods and to relate the conformational effects induced by these modifications at the oligomer level by using MD simulations studies. Accordingly, monomer level studies were performed on LNA, BNA modifications and oligomer level studies on 14-mer duplex gapmers, wherein, a 5′-CTTAGCACTGGCCT-3′ nucleic acid strand was built by incorporating the LNA, BNA modifications selectively at the two terminal residues while the remaining residues being PS-DNA nucleotides. The PS-DNA segment in the duplexes will allow RNase H activation and protein binding facilitating tissue distribution while non-RNase H activating segment containing the LNA, BNA residues will provide increased nucleolytic stability, affinity to target RNAs with decreased polyanionic characteristics.

According to the molecular level investigation, insertion of the particular antisense modifications had no inconvenience on the *N-type* sugar puckering maintaining relative sugar-base orientation in the *anti*-conformation which can strengthen the base pairing, stacking interactions in favour of RNA-mimicking conformations. Modifications on the guanine nucleobases are predicted to be better electron donors and modifications on the thymine nucleobases are predicted to be better electron acceptors. The HOMO-LUMO isosurfaces of all the monomer nucleotides were majorly distributed on the nucleobase region irrespective of the modifications, be it the purines or pyrimidines. MO isosurfaces being embedded into the nucleobase region might be one of the prime reasons in dropping their interactions with the cellular endonuclease RNase H. On the contrary, if the MO isosurfaces are well distributed into the modified bridging unit, the same will be highly available to the surrounding environment for various electron-exchange processes which may aid in the interaction with the RNase H and thereby increase their antisense activity.

The present work also concentrates on the derivation of the global reactivity descriptors global hardness (η), global softness (S), chemical potential (μ) and electrophilicity (ω) of the titled monomer nucleotides. Global hardness and softness suggest that irrespective of the type of antisense alterations, guanine nucleobases will be chemically less active in electron receiving and elimination processes during a chemical reaction and hence less soft and alterations on 5-methylcytosine nucleobases will be chemically more active in the respective electron receiving and elimination processes and hence softer compared to the alterations on the other nucleobases. Chemical potential suggests alterations on thymine nucleobase have more negative chemical potential and alterations on the guanine nucleobase have less negative chemical potential. Electrophilicity also suggest that alterations on guanine nucleobases are less electrophilic which is because guanine nucleobases have high lying E_{LUMO} and will accept electrons less easily, hence less electrophillic. On the other hand, alterations on the thymine nucleobases are more electrophilic, because thymine nucleobases have low lying E_{LUMO} and will accept electrons more easily and hence more electrophilic. Overall, the LNA, BNA and the PS modified LNA, BNA antisense alterations on the purine nucleobases have less negative chemical potential and are less electrophillic compared to modifications on the pyrimidine nucleobases.

However, stability of oligomer duplexes depends on several factors like the purine-pyrimidine content, oligomer sequence-dependencies, backbone conformation, base-pairing interactions, binding energies and solvation of duplex oligomers as a whole. Accordingly, the duplex dynamic structures, intra-strand and inter-strand distances, sugar-puckering, *N-glycosidic* torsion angles, backbone flexibility all were preferring an intermediate structure between RNA-mimicking *A-form* and DNA-mimicking *B-form* duplexes. The non-terminal residues in the ASO strands were majorly *B-type* which can activate the RNase H and the terminal residues were *A-type* which can improve the nuclease resistance and target binding affinity. However, the RNA strands were oscillating between an *A-form* and *B-form* conformation.

It is well-established that bulk properties of oligomers are strongly governed by the chemical properties of their monomers. Hence, oligomer structural properties of the modified ASO/RNA duplexes were studied in association with electronic properties of the LNA, BNA monomer nucleotides. MO analysis from molecular level calculations predicted MO iso-surfaces of the LNA, BNA monomer nucleotides to be majorly distributed on the nucleobase region. MO-isosurfaces of the LNA, BNA monomer nucleotides being embedded in the nucleobase region suggests that upon duplex formation with target RNAs, the non-RNase H activating segment of the duplexes would be less available for various electron-exchange processes. Thus, to design novel BNA modifications one can opt for developing BNA modifications with MO-isosurfaces distributed in the modified bridging unit over BNA modifications with MO-isosurfaces located in the nucleobase region. Also, for the particular sequence considered solvation of the duplexes although were higher compared to the natural oligonucleotides, their binding energies being relatively lower may lead to decreased antisense activity. Because gapmers modified with LNAs has been reported of potent knockdown activity with hepatotoxic side effects, based on our presumptions the BNA gapmers with similar drawbacks as the LNAs will further keep causing hepatotoxic side effects as LNA gapmers.

A combined monomer- and oligomer-based study as such has helped in understanding structure-activity relationship of the LNA, BNA modifications and has also yielded a systematic DFT & MD method-based paradigm for fine tuning the LNA, BNA modifications to obtain beneficial antisense modifications.

Bibliography

[1] Chan, J. H., Lim, S., and Wong, W. F. Antisense oligonucleotides: from design to therapeutic application. *Clinical and Experimental Pharmacology and Physiology*, 33:533-540, 2009.

[2] Crooke, S.T. ed. Antisense drug technology: principles, strategies, and applications. CRC press, 2007.

[3] Bennett, C. F., and Swayze, E. E. RNA targeting therapeutics: molecular mechanisms of antisense oligonucleotides as a therapeutic platform. *Annual Review of Pharmacology and Toxicology*, 50(1):259-293, 2010.

[4] Zamaratski, E., Pradeepkumar, P. I., and Chattopadhyaya, J. A critical survey of the structure-function of the antisense oligo/RNA hetero duplex as substrate for RNase H. *Journal of Biochemical and Biophys*ical *Methods*, 48(3):189-208, 2001.

[5] Nowotny, M., Gaidamakov, S. A., Ghirlando, R., Cerritelli, S. M., Crouch, R. J., and Yang, W. Structure of human RNase H1 complexed with an RNA/DNA hybrid: insight into HIV reverse transcription. *Molecular Cell*, 28(2):264-276, 2007.

[6] Herbert, C., Dzowo, Y. K., Urban, A., Kiggins, C. N., and Resendiz, M. J. Reactivity and specificity of RNase T1, RNase A, and RNase H toward oligonucleotides of RNA containing 8-Oxo-7, 8-dihydroguanosine. *Biochemistry*, 57(20):2971-2983, 2018.

[7] Kurreck, J. Antisense technologies: improvement through novel chemical modifications. *European Journal Biochem*istry, 270(8):1628-1644, 2003.

[8] Moss, K. H., Popova, P., Hadrup, S. R., Astakhova, K., and Taskova, M. Lipid nanoparticles for delivery of therapeutic RNA oligonucleotides. *Molecular Pharmaceutics*, 16(6):2265-2277, 2019.

[9] Gheibi-Hayat, S. M., and Jamialahmadi, K. Antisense Oligonucleotide (AS-ODN) Technology: Principle, Mechanism and Challenges. *Biotechnology and Applied Biochemistry*, 68(5):1086-1094, 2021.

[10] The Vitravene Study Group, A randomized controlled clinical trial of intravitreous fomivirsen for treatment of newly diagnosed peripheral cytomegalovirus retinitis in patients with AIDS. *American Journal of Ophthalmology*, 133(4):467-474, 2002.

[11] Le Calvez, H., Yu, M., and Fang, F. Biochemical prevention and treatment of viral infections–A new paradigm in medicine for infectious diseases. *Virology Journal*, 1(12):1-6, 2004.

[12] Stein, C. A., and Castanotto, D. FDA-approved oligonucleotide therapies in 2017. *Molecular Therapy*, 25(5):1069-1075, 2017.

[13] Silva, A. C., Lobo, D. D., Martins, I. M., Lopes, S. M., Henriques, C., Duarte, S. P., Dodart, J. C., Nobre, R. J., and Pereira de Almeida, L. Antisense oligonucleotide therapeutics in neurodegenerative diseases: the case of polyglutamine disorders. *Brain*, 143(2):407-429, 2020.

[14] Takei, Y., Kadomatsu, K., Yuzawa, Y., Matsuo, S., and Muramatsu, T. A small interfering RNA targeting vascular endothelial growth factor as cancer therapeutics. *Cancer Research*, 64(10):3365-3370, 2004.

[15] Gong, M., Lu, Z., Fang, G., Bi, J., and Xue, X. A small interfering RNA targeting osteopontin as gastric cancer therapeutics. *Cancer Letters*, 272(1):148-159, 2008.

[16] Kiełpiński, Ł. J., Hagedorn, P. H., Lindow, M., and Vinther, J. RNase H sequence preferences influence antisense oligonucleotide efficiency. *Nucleic Acids Research*, 45(22):12932-12944, 2017.

[17] Hagedorn, P. H., Pontoppidan, M., Bisgaard, T. S., Berrera, M., Dieckmann, A., Ebeling, M., Møller, M. R., Hudlebusch, H., Jensen, M. L., Hansen, H. F., Koch, T., and Lindow, M. Identifying and avoiding off-target effects of RNase H-dependent antisense oligonucleotides in mice. *Nucleic Acids Research*, 46(11):5366-5380, 2018.

[18] Campbell, J. M., Bacon, T. A., and Wickstrom, E. Oligodeoxynucleoside phosphorothioate stability in subcellular extracts, culture media, sera and cerebrospinal fluid. *Journal of Biochemical and Biophysical Methods*, 20(3):259-267, 1990.

[19] Zhang, R., Diasio, R. B., Lu, Z., Liu, T., Jiang, Z., Galbraith, W. M., and Agrawal, S. Pharmacokinetics and tissue distribution in rats of an oligodeoxynucleotide phosphorothioate (GEM 91) developed as a therapeutic agent for human immunodeficiency virus type-1. *Biochemical Pharmacology*, 49(7):929-939, 1995.

[20] Agrawal, S., Goodchild, J., Civeira, M., Sarin, P. S., and Zamecnik, P. C. Phosphoramidate, phosphorothioate, and methylphosphonate analogs of oligodeoxynucleotide: inhibitors of replication of human immunodeficiency virus. *Nucleosides and Nucleotides*, 8(5-6):819-823, 1989.

[21] Iwamoto, N., Butler, D. C., Svrzikapa, N., Mohapatra, S., Zlatev, I., Sah, D. W., Meena, Standley, S. M., Lu, G., Apponi, L. H., Frank-Kamenetsky, M., Zhang, J. J.,

Vargeese, C., and Verdine, G. L. Control of phosphorothioate stereochemistry substantially increases the efficacy of antisense oligonucleotides. *Nature Biotechnology*, 35(9):845-851, 2017.

[22] Shen, W., De Hoyos, C. L., Migawa, M. T., Vickers, T. A., Sun, H., Low, A., Bell, T.A., Rahdar, M., Mukhopadhyay, S., Hart, C. E., Bell, M., Riney, S., Murray, S. F., Greenlee, S., Crooke, R. M., Liang, X., Seth, P. P., and Crooke, S. T. Chemical modification of PS-ASO therapeutics reduces cellular protein-binding and improves the therapeutic index. *Nature Biotechnology*, 37(6):640-650, 2019.

[23] Manoharan, M. 2′-Carbohydrate modifications in antisense oligonucleotide therapy: importance of conformation, configuration and conjugation. *Biochimica et Biophysica Acta (BBA)-Gene Structure and Expression*, 1489(1):117-130, 1999.

[24] Herdewijn, P. Conformationally restricted carbohydrate-modified nucleic acids and antisense technology. *Biochimica et Biophysica Acta (BBA)-Gene Structure and Expression*, 1489(1):167-179, 1999.

[25] Finn, P. J., Gibson, N. J., Fallon, R., Hamilton, A., and Brown, T. Synthesis and properties of DNA-PNA chimeric oligomers. *Nucleic Acids Research*, 24(17):3357-3363, 1996.

[26] Rosie, Z.Y., Kim, T.W., Hong, A., Watanabe, T. A., Gaus, H. J., and Geary, R.S. Cross-species pharmacokinetic comparison from mouse to man of a second-generation antisense oligonucleotide, ISIS 301012, targeting human apolipoprotein B-100. *Drug Metabolism and Disposition*, 35(3):460-468, 2007.

[27] Geary, R. S., Wancewicz, E., Matson, J., Pearce, M., Siwkowski, A., Swayze, E., and Bennett, F. Effect of dose and plasma concentration on liver uptake and pharmacologic activity of a 2′-methoxyethyl modified chimeric antisense oligonucleotide targeting PTEN. *Biochemical Pharmacology*, 78(3):284-291, 2009.

[28] Post, N., Yu, R., Greenlee, S., Gaus, H., Hurh, E., Matson, J., and Wang, Y. Metabolism and disposition of volanesorsen, a 2′-O-(2 methoxyethyl) antisense oligonucleotide, across species. *Drug Metabolism and Disposition*, 47(10):1164-1173, 2019.

[29] Singh, S. K., Koshkin, A. A., Wengel, J., and Nielsen, P. LNA (locked nucleic acids): synthesis and high-affinity nucleic acid recognition. *Chemical Communications*, (4):455-456, 1998.

[30] Abdur Rahman, S. M., Seki, S., Obika, S., Yoshikawa, H., Miyashita, K., and Imanishi, T. Design, Synthesis, and Properties of 2 ‘,4 ‘-BNA^{NC}: A Bridged Nucleic Acid Analogue. *Journal of Am*erican *Chemical Soc*iety, 130(14):4886-4896, 2008.

[31] Shrestha, A. R., Kotobuki, Y., Hari, Y., and Obika, S. Guanidine bridged nucleic acid (GuNA): an effect of a cationic bridged nucleic acid on DNA binding affinity. *Chemical Communications*, 50(5):575-577, 2014.

[32] Langner, H. K., Jastrzebska, K., and Caruthers, M. H. Synthesis and characterization of thiophosphoramidate morpholino oligonucleotides and chimeras. *Journal of the Am*erican *Chemical Society*, 142(38):16240-16253, 2020.

[33] Fluiter, K., ten Asbroek, A. L., de Wissel, M. B., Jakobs, M. E., Wissenbach, M., Olsson, H., Olsen, O., Oerum, H., and Baas, F. In vivo tumor growth inhibition and biodistribution studies of locked nucleic acid (LNA) antisense oligonucleotides. *Nucleic Acids Research*, 31(3):953-962, 2003.

[34] Darfeuille, F., Hansen, J. B., Orum, H., Primo, C. D., and Toulmé, J. J. LNA/DNA chimeric oligomers mimic RNA aptamers targeted to the TAR RNA element of HIV-1. *Nucleic Acids Research*, 32(10):3101-3107, 2004.

[35] Laxton, C., Brady, K., Moschos, S., Turnpenny, P., Rawal, J., Pryde, D. C., Sidders, B., Corbau, R., Pickford, C., and Murray, E. J. Selection, optimization, and pharmacokinetic properties of a novel, potent antiviral locked nucleic acid-based antisense oligomer targeting hepatitis C virus internal ribosome entry site. *Antimicrobial Agents and Chemotherapy*, 55(7):3105-3114, 2011.

[36] Swayze, E. E., Siwkowski, A. M., Wancewicz, E. V., Migawa, M. T., Wyrzykiewicz, T. K., Hung, G., Monia, B. P., and Bennett, A. C. F. Antisense oligonucleotides containing locked nucleic acid improve potency but cause significant hepatotoxicity in animals. *Nucleic Acids Research*, 35(2):687-700, 2007.

[37] Seth, P. P., Siwkowski, A., Allerson, C. R., Vasquez, G., Lee, S., Prakash, T. P., Wancewicz, E. V., Witchell, D., and Swayze, E. E. Short antisense oligonucleotides with novel 2′− 4′ conformationaly restricted nucleoside analogues show improved potency without increased toxicity in animals. *Journal of Medicinal Chemistry*, 52(1):10-13, 2009.

[38] Seth, P. P., Vasquez, G., Allerson, C. A., Berdeja, A., Gaus, H., Kinberger, G. A., Prakash, T. P., Migawa, M. T., Bhat, B., and Swayze, E. E. Synthesis and biophysical evaluation of 2′, 4′-constrained 2′ O-methoxyethyl and 2′, 4′-constrained

2′ O-ethyl nucleic acid analogues. *The Journal of Organic Chemistry*, 75(5):1569-1581, 2010.

[39] Prakash, T. P., Siwkowski, A., Allerson, C. R., Migawa, M. T., Lee, S., Gaus, H. J., Black, C., Seth, P.P., Swayze, E. E., and Bhat, B. Antisense oligonucleotides containing conformationally constrained 2′, 4′-(N-methoxy) aminomethylene and 2′, 4′-aminooxymethylene and 2′-O, 4′-C-aminomethylene bridged nucleoside analogues show improved potency in animal models. *Journal of Medicinal Chemistry*, 53(4):1636-1650, 2010.

[40] Yamamoto, T., Yasuhara, H., Wada, F., Harada-Shiba, M., Imanishi, T., and Obika, S. Superior silencing by 2′,4′-BNA^{NC}-based short antisense oligonucleotides compared to 2′,4′-BNA/LNA-based apolipoprotein B antisense inhibitors. *Journal of Nucleic Acids*, 2012.

[41] Natsume, T., Ishikawa, Y., Dedachi, K., Tsukamoto, T., and Kurita, N. DFT study of the electronic properties of DNA–DNA and PNA–DNA double strands. *International Journal of Quantum Chemistry*, 106(15):3278-3287, 2006.

[42] Uppuladinne, M.V., Jani, V., Sonavane, U. B., and Joshi, R. R. Quantum chemical studies of novel 2′-4′ conformationally restricted antisense monomers. *International Journal of Quantum Chemistry*, 113(23):2523-2533, 2013.

[43] Bhai, S., and Ganguly, B. Role of backbones on the interaction of metal ions with deoxyribonucleic acid and peptide nucleic acid: A DFT study. *Journal of Molecular Graphics and Modelling*, 93:107445, 2019.

[44] Uppuladinne, M.V., Sonavane, U. B., Deka, R. C., and Joshi, R. R. Structural insight into antisense gapmer-RNA oligomer duplexes through molecular dynamics simulations. *Journal of Biomolecular Structure and Dynamics*, 37(11):2823-2836, 2019.

[45] Galindo-Murillo, R., Cohen, J. S., and Akabayov, B. Molecular dynamics simulations of acyclic analogs of nucleic acids for antisense inhibition. *Molecular Therapy Nucleic Acids*, 23:527-535, 2021.

[46] Hansen, H. F., Albaek, N., Hansen, B. R., Shim, I., Bohr, H., and Koch, T. In vivo uptake of antisense oligonucleotide drugs predicted by ab initio quantum mechanical calculations. *Scientific Reports*, 11:1-13, 2021.

[47] Uppuladinne, M.V., Dowerah, D., Sonavane, U. B., Ray, S. K., Deka, R. C., and Joshi, R. R. Structural Insight into Locked Nucleic Acid based Novel Antisense

Modifications: A DFT calculations at monomer and MD simulations at oligomer level. *Journal of Molecular Graphics and Modellig*, 107:945, 2021.

[48] Kondo, J., Nomura, Y., Kitahara, Y., Obika, S., and Torigoe, H. The crystal structure of a 2′,4′-BNA^{NC}[N–Me]-modified antisense gapmer in complex with the target RNA. *Chemical Communications*, 52(11):2354-2357, 2016.

[49] Frisch, M. J., Trucks, G.W., Schlegel, H. B., Scuseria, G. E., Robb, M. A., Cheeseman, J. R., Scalmani, G., Barone, V., Mennucci, B., Petersson, G. A., Nakatsuji, H., Li, X., Caricato, M., Marenich, A. V., Bloino, J., Janesko, B. G., Gomperts, R., Mennucci, B., Hratchian, H. P., Ortiz, J. V., Izmaylov, A. F., Sonnenberg, J. L., Williams-Young, D., Ding, F., Lipparini, F., Egidi, F., Goings, J., Peng, B., Petrone, A., Henderson, T., Ranasinghe, D., Zakrzewski, V. G., Gao, J., Rega, N., Zheng, G., Liang, W., Hada, M., Ehara, M., Toyota, K., Fukuda, R., Hasegawa, J., Ishida, M., Nakajima, T., Honda, Y., Kitao, O., Nakai, H., Vreven, T., Throssell, K., Montgomery, J. A. Jr., Peralta, J. E., Ogliaro, F., Bearpark, M. J., Heyd, J. J., Brothers, E. N., Kudin, K. N., Staroverov, V. N., Keith, T. A., Kobayashi, R., Normand, J., Raghavachari, K., Rendell, A. P., Burant, J. C., Iyengar, S. S., Tomasi, J., Cossi, M., Millam, J. M., Klene, M., Adamo, C., Cammi, R., Ochterski, J. W., Martin, R. L., Morokuma, K., Farkas, O., Foresman, J. B., Fox, D. J. Gaussian 09, Revision D. 01, *Gaussian, Inc.*, Wallingford CT, 2009.

[50] BIOVIA, Dassault Systèmes, [Discovery Studio], [Client version 19.1.0], San Diego: Dassault Systèmes, 2019.

[51] Hehre, W. J., Ditchfield, R., and Pople, J. A. Self—consistent molecular orbital methods. XII. Further extensions of Gaussian—type basis sets for use in molecular orbital studies of organic molecules. *The Journal of Chemical Physics*, 56(5):2257-2261, 1972.

[52] Hariharan, P. C., and Pople, J. A. The influence of polarization functions on molecular orbital hydrogenation energies. *Theoretica Chimica Acta*, 28:213-222, 1973.

[53] Zhao, Y., and Truhlar, D. G. The M06 suite of density functionals for main group thermochemistry, thermochemical kinetics, noncovalent interactions, excited states, and transition elements: two new functionals and systematic testing of four M06-class functionals and 12 other functionals. *Theoretical Chemistry Accounts*, 120:215-241, 2008.

[54] Takano, Y., and Houk, K. N. Benchmarking the conductor-like polarizable continuum model (CPCM) for aqueous solvation free energies of neutral and ionic organic molecules. *Journal of Chemical Theory and Computation*, 1(1):70-77, 2005.

[55] Lu, T., and Chen, F. Multiwfn: a multifunctional wavefunction analyzer. *Journal of Computational Chemistry*, 33(5):580-592, 2012.

[56] Parr, R. G., and Yang, W. Density functional approach to the frontier-electron theory of chemical reactivity. *Journal of American Chemical Society*, 106(14):4049-4050, 1984.

[57] Luo, J., Xue, Z. Q., Liu, W. M., Wu, J. L., and Yang, Z. Q. Koopmans' theorem for large molecular systems within density functional theory. The *Journal of Physical Chemistry A*, 110(43):12005-12009, 2006.

[58] Vijayaraj, R., Subramanian, V., and Chattaraj, P.K. Comparison of global reactivity descriptors calculated using various density functionals: a QSAR perspective. *Journal of Chemical Theory and Computation*, 5(10):2744-2753, 2009.

[59] Cornell, W. D., Cieplak, P., Bayly, C. I., Gould, I. R., Merz, K. M., Ferguson, D. M., Spellmeyer, D. C., Fox, T., Caldwell, J. W., and Kollman, P. A. A second generation force field for the simulation of proteins, nucleic acids, and organic molecules. *Journal of the American Chemical Society*, 117(19):5179-5197, 1995.

[60] Pérez, A., Marchán, I., Svozil, D., Sponer, J., Cheatham III, T. E., Laughton, C. A., and Orozco, M. Refinement of the AMBER force field for nucleic acids: improving the description of α/γ conformers. *Biophysical Journal*, 92(11):3817-3829, 2007.

[61] Case, D. A., Ben-Shalom, I. Y., Brozell, S. R., Cerutti, D. S., Cheatham III, T. E., Cruzeiro, V. W. D., Darden T. A., Duke R. E., Ghoreishi D., Gilson M. K., Gohlke H., Goetz A. W., Greene D., Harris R, Homeyer N., Huang Y., Izadi S., Kovalenko A., Kurtzman T., Lee T. S., LeGrand S., Li P., Lin C., Liu J., Luchko T., Luo R., Mermelstein D. J., Merz K. M., Miao Y., Monard G., Nguyen C., Nguyen H., Omelyan I., Onufriev A., Pan F., Qi R., Roe D. R., Roitberg A., Sagui C., Schott-Verdugo S., Shen J., Simmerling C. L., Smith J., SalomonFerrer R., Swails J., Walker R. C., Wang J., Wei H., Wolf R. M., Wu X., Xiao L., York D. M. and Kollman P. A. AMBER 2018, University of California, San Francisco, 2018.

[62] Genna, V., Iglesias-Fernández, J., Reyes-Fraile, L., Villegas, N., Guckian, K., Seth, P., Wan, B., Cabrero, C., Terrazas, M., Brun-Heath, I., González, C., Sciabola, S., Villalobos, A., and Orozco, M. Controlled sulfur-based engineering confers

mouldability to phosphorothioate antisense oligonucleotides. *Nucleic Acids Research*, 51(10):4713-4725, 2023.

[63] Jorgensen, W. L., Chandrasekhar, J., Madura, J. D., Impey, R. W., and Klein, M. L. Comparison of simple potential functions for simulating liquid water. The *Journal of Chemical Physics*, 79(2):926-935, 1983.

[64] Machireddy, B., Kalra, G., Jonnalagadda, S., Ramanujachary, K., and Wu, C. Probing the binding pathway of BRACO19 to a parallel-stranded human telomeric G-quadruplex using molecular dynamics binding simulation with AMBER DNA OL15 and ligand GAFF2 force fields. *Journal of Chemical Information and Modeling*, 57(11):2846-2864, 2017.

[65] Zhao, J., Kennedy, S. D., and Turner, D. H. Nuclear Magnetic Resonance Spectra and AMBER OL3 and ROC-RNA Simulations of UCUCGU Reveal Force Field Strengths and Weaknesses for Single-Stranded RNA. *Journal of Chemical Theory and Computation*, 18(2):1241-1254, 2022.

[66] Cheatham, T. I., Miller, J. L., Fox, T., Darden, T. A., and Kollman, P. A. Molecular dynamics simulations on solvated biomolecular systems: the particle mesh Ewald method leads to stable trajectories of DNA, RNA, and proteins. *Journal of the American Chemical Society*, 117(14):4193-4194, 1995.

[67] Miyamoto, S., and Kollman, P. A. Settle: An analytical version of the SHAKE and RATTLE algorithm for rigid water models. *Journal of Computational Chemistry*, 13(8):952-962, 1992.

[68] Roe, D. R., and Cheatham III, T. E. PTRAJ and CPPTRAJ: software for processing and analysis of molecular dynamics trajectory data. *Journal of Chemical Theory and Computation*, 9(7):3084-3095, 2013.

[69] Alden, C. J., and Kim, S. H. Solvent-accessible surfaces of nucleic acids. *Journal of molecular biology*, 132(3): 411-434, 1979.

[70] Xu, L., Sun, H., Li, Y., Wang, J., and Hou, T. Assessing the performance of MM/PBSA and MM/GBSA methods. 3. The impact of force fields and ligand charge models. The *Journal of Physical Chemistry B*, 117(28):8408-8421, 2013.

[71] Golyshev, V. M., Pyshnyi, D. V., and Lomzov, A. A. Calculation of Energy for RNA/RNA and DNA/RNA Duplex Formation by Molecular Dynamics Simulation. *Molecular Biology*, 55(6):927-940, 2021.

[72] Zhang, Z., Vogele, J., Mráziková, K., Kruse, H., Cang, X., Wöhnert, J., Krepl, M., and Sponer, J. Phosphorothioate substitutions in RNA structure studied by molecular dynamics simulations, QM/MM calculations, and NMR experiments. *The Journal of Physical Chemistry B*, 125(3):825-840, 2021.

[73] Heinemann, U., and Roske, Y. Symmetry in nucleic-acid double helices. *Symmetry*, 12(5):737, 2020.

[74] Levitt, M., and Warshel, A. Extreme conformational flexibility of the furanose ring in DNA and RNA. *Journal of the American Chemical Society*, 100(9):2607-2613, 1978.

[75] Pande, V., and Nilsson, L. Insights into structure, dynamics and hydration of locked nucleic acid (LNA) strand-based duplexes from molecular dynamics simulations. *Nucleic Acids Research*, 36(5):1508-1516, 2008.

[76] Ho, P. S., and Carter, M. DNA structure: Alphabet soup for the cellular soul. *In DNA Replication-Current Advances*, IntechOpen, 2011.

[77] Xia, Z., Bell, D. R., Shi, Y., and Ren, P. RNA 3D structure prediction by using a coarse-grained model and experimental data. *The Journal of Physical Chemistry B*, 117(11):3135-3144, 2013.

[78] Noy, A., Luque, F.J., and Orozco, M. Theoretical analysis of antisense duplexes: determinants of the RNase H susceptibility. *Journal of the American Chemical Society*, 130(11):3486-3496, 2008.

[79] Sponer, J., Zgarbová, M., Jurecka, P., Riley, K. E., Sponer, J. E., and Hobza, P. Reference quantum chemical calculations on RNA base pairs directly involving the 2′-OH group of ribose. *Journal of Chemical Theory and Computation*, 5(4):1166-1179, 2009.

[80] Butcher, S. E., and Pyle, A. M. The molecular interactions that stabilize RNA tertiary structure: RNA motifs, patterns, and networks. *Accounts of Chemical Research*, 44(12):1302-1311, 2011.

[81] Yakovchuk, P., Protozanova, E., and Frank-Kamenetskii, M. D. Base-stacking and base-pairing contributions into thermal stability of the DNA double helix. *Nucleic Acids Research*, 34(2):564-574, 2006.

[82] Parker, T. M., Hohenstein, E. G., Parrish, R. M., Hud, N. V., and Sherrill, C. D. Quantum-mechanical analysis of the energetic contributions to π stacking in nucleic

acids versus rise, twist, and slide. *Journal of the American Chemical Society*, 135(4):1306-1316, 2013.

[83] Chen, F., Sun, H., Wang, J., Zhu, F., Liu, H., Wang, Z., Lei, T., Li, Y., and Hou, T. Assessing the performance of MM/PBSA and MM/GBSA methods. 8. Predicting binding free energies and poses of protein–RNA complexes. *RNA*, 24(9):1183-1194, 2018.